TÉCNICO LISBOA

Design of an Energy Storage System for the Tokamak ISTTOK

Pedro Miguel de Castro Pena Brandão Rodrigues

Thesis to obtain the Master of Science Degree in

Electrical and Computer Engineering

Supervisor: Prof. José Fernando Alves da Silva

Examination Committee

Chairperson: Prof. Célia Maria Santos Cardoso de Jesus
Supervisor: Prof. José Fernando Alves da Silva
Member of the Committee: Prof. Horácio João Matos Fernandes

November 2021

Declaration

I declare that this document is an original work of my own authorship and that it fulfills all the requirements of the Code of Conduct and Good Practices of the Universidade de Lisboa.

Acknowledgments

I would like to express my deep gratitude to Professor José Fernando Alves da Silva my supervisor who has carefully verified and assisted my work. For his guidance and the time he dedicated to me, I give him my sincere appreciation. Without his help and contribution, this work would have not been possible.

I also wish to thank my family and my friends for all the support and encouragement throughout my entire life. For never doubting me, and helping me get where I am today.

Abstract

The present thesis addresses the design of an energy storage system (ESS) for the research fusion device ISTTOK. The purpose of this work is to study, simulate and design a supplement for this tokamak, which has an operation cycle characterized by a pulse of 3 s and a rest period of approximately 15 min. The system is designed to supply the coils that produce the toroidal magnetic field (MF), used for plasma confinement, but also to retrieve most of the energy stored in these coils during the operation, avoiding the re-injection of this energy into the public grid. The solutions developed are compared based on their functionalities and requirements, lastly, the feasibility of each is accessed.

The data and features of the tokamak ISTTOK are presented, with special emphasis on the toroidal field (TF) system. The existing 1 MVA thyristor based power supply is studied, and a precise analysis and simulation of the system is made using Matlab and Simulink. New energy recovery resonant converter topologies are proposed, to be able to cope with currents near 10 kA.

The most appropriate energy storage technologies (ESTs) are discussed and compared based on their general characteristics, performance, and application to this specific case. The suitable energy storage systems analyzed are high power density batteries, flywheels, capacitors and supercapacitors, which in this case appears to be the most promising technology. The cells and semiconductor devices currently available on the market are also presented.

Keywords

Tokamak, Energy Storage, Power supply, Supercapacitors, Toroidal Field

Resumo

O presente trabalho descreve o projeto de um sistema de armazenamento de energia para o dispositivo experimental de fusão nuclear ISTTOK. O propósito deste trabalho é estudar, simular e dimensionar um sistema suplementar para este *tokamak*, que tem um ciclo de operação caracterizado por 3 s de impulso e 15 min de repouso. O sistema é concebido para alimentar as bobinas que produzem o campo magnético toroidal, responsável por confinar o plasma, mas também reaproveitar parte da energia armazenada nestas bobinas durante a operação, evitando que esta seja injetada na rede publica. As soluções desenvolvidas são comparadas com base nas suas funcionalidades e requisitos, sendo a sua viabilidade avaliada.

As características do tokamak ISTTOK são apresentadas, com particular destaque no sistema que produz o campo toroidal. A fonte de alimentação existente, de 1 MVA baseada em tiristores, também é alvo de estudo, assim, será realizada uma análise precisa e o sistema será simulado usando os programas Simulink e MATLAB. São propostas novas topologias de conversores ressonantes para recuperação de energia, capazes de lidar com correntes próximas de 10kA.

As tecnologias de armazenamento de energia mais apropriadas são discutidas e comparadas com base nas características, desempenho e aplicação a este caso. Os sistemas de armazenamento mais adequados são as baterias de alta densidade de potência, *flywheels*, condensadores e supercondensadores, que neste caso aparenta ser a tecnologia mais efetiva. As células e dispositivos semiconductores disponíveis no mercado também são apresentados.

Palavras Chave

Tokamak, Armazenamento de energia, Fonte de Alimentação, Supercondensadores, Campo Toroidal

Contents

List of Figures

List of Tables

List of Acronyms

AC Alternating Current

BMS Battery Management System

CB Capacitor Bank

CC Capacitor Cell

DC Direct Current

ECB Electrolytic Capacitor Bank

EDP Energias de Portugal

ESR Equivalent Series Resistance

ESS Energy Storage System

EST Energy Storage Technology

FESS Flywheel energy storage systems

IGBT Insulated-Gate Bipolar Transistor

ISTTOK Instituto Superior Técnico TOKamak

ITER International Thermonuclear Experimental Reactor

MF Magnetic Field

PI Proportional Integral

SCR Silicon Controlled Rectifier

SOC State of Charge

TF Toroidal Field

TORTUR TORus for TURbulent

UPS Uninterruptible Power Supply

1

Introduction

Contents

1.1 Motivation

The application of nuclear fusion energy for power generation is becoming more prevalent as a subject of study and experiment. The increasing power demand and energy consumption have to be supported by existing electrical grids. Nuclear fusion has great potential due to the large amount of energy released on nuclear reactions, however, the process of transforming this energy into electrical energy is extremely challenging and complex. The technology and knowledge to assemble sustainable nuclear fusion power plants are still lacking. Nevertheless, the viability of this process is being assessed.

Currently, tokamaks are the main candidates for nuclear fusion reactors. The final decision on the feasibility and future applications of tokamaks will be based on the operation of ITER (International Thermonuclear Experimental Reactor) in pre-burning plasma regime [1]. Unfortunately, the prediction for the project completion is around 2030 to 2035. With that being said, smaller tokamaks are also important for nuclear fusion studies. Estimates and predictions are performed based on the available information of existing tokamaks, as a result, experiments conducted in small reactors are crucial to study plasma behaviour [1].

ISTTOK is a small tokamak at the research center CFN (Centro de Fusão Nuclear) of IST (Instituto Superior Técnico), with a circular cross-section and an iron core transformer. The toroidal field (TF) system requires high current for the coils, as a result, the leftover energy stored on this inductor is significant. Unfortunately, this remaining energy is not reused in the tokamak, instead, it is injected back into the public grid, causing minor disturbances and power quality issues. Consequently, EDP (Energias de Portugal) charges this re-injected energy as reactive energy. The solution for this problem is to store, after the operation, the remaining energy into an energy storage system (ESS). This work addresses the design of this ESS.

Energy storage technologies (ESTs) are developing rapidly. They are acknowledged as an essential element in the modern energy supply chain [2]. The application of EST might lead to sustainable energy systems. One of the main applications is to renewable energy sources where several fluctuations occur in the generation, which makes them unreliable for steady energy supply. This unbalanced between supply and demand can be compensated with energy storage [3]. Other benefits of ESSs are the improvement of the efficiency on this systems, the enhancement of grid stability and the reduction of the environmental impact of energy generation [2]. In conclusion, ESTs are capable of storing the excess energy generated so it can be later converted into useful energy.

1.2 Objectives

This work addresses the design of an ESS, based on supercapacitors, for the TF coils of the ISTTOK. Considering this main goal the following objectives are established:

- To revise the state-of-the-art, with special regard to energy storage technologies;
- To examine the products currently available on the market, regarding semiconductor devices and different types of cells including supercapacitors and electrolytic capacitors;
- To review the documentation of the existing TF power supply and to simulate this system;
- To analyse possible solutions for the energy storage system.
- To design the supercapacitor and electrolytic capacitor banks;
- To discuss the results and simulations obtained with MATLAB and Simulink;
- To compare the solutions that were accessed and to draw conclusions;

1.3 Dissertation Outline

This thesis is structured in 5 chapters. Chapter 1 gives a brief introduction and presents the main objectives of the work. Chapter 2 provides an overview of the current state-of-the-art, and specifies the data and parameters of the elements that are part of the system. Chapter 3 describes the implementation of the existing TF power supply, and presents the results and simulations of this system. Chapter 4 covers the possible solutions for the energy storage system, including the simulations obtained. Lastly, ifn Chapter 5 the solutions proposed are compared taking into consideration the advantages and requirements, and the final conclusions are reported along with proposed future developments.

2

State-of-the-art

Contents

2.1 Introduction

This chapter gives the theoretical background needed for this work. The problem is presented and possible solutions regarding the energy storage system are studied and compared through the analysis of similar published work. A brief introduction of tokamaks is made, with emphasis on the ISTTOK. The existing power supply of the TF coils is described in detail. The energy storage technologies are discussed and compared considering the main characteristics, advantages and possible application to the energy storage system of the ISTTOK. The storage cells and semiconductor devices available in the market are presented, and their parameters specified. A brief description of resonant circuits is also made.

2.2 Tokamaks

There are two types of nuclear reactions used to produce electrical energy, fission and fusion. In both of them, there is a transformation of at least one nuclide and huge amounts of energy are released in this process. In nuclear fission a heavy nucleus is split into smaller nuclei, in nuclear fusion, two or more light nuclei combine to form a single heavier nucleus [4]. The first fusion machine considered to be a Tokamak was assembled in the 1950s, at the Kurchatov Institute of Moscow [5]. The term tokamak is a transliteration of a Russian expression meaning toroidal chamber with magnetic coils. ITER (International Thermonuclear Experimental Reactor) is an ongoing project which will be the largest tokamak in the world. This reactor is intended to evaluate the feasibility and future applications of tokamaks. The main goal is to produce more thermal power, than the power used to heat the plasma, hence producing net power [1].

Basic Principles of Operation

Tokamak reactors are devices capable of confining hot plasmas through strong magnetic fields in the shape of a torus, thus creating conditions for nuclear fusion to be possible. This type of magnetic confinement is used to produced controlled thermonuclear fusion. There are other candidates for fusion reactors but Tokamaks are currently the leading ones [6].

The Tokamak operation is based on the interaction between magnetic fields and plasma. This state of matter is electrically conductive, therefore can be manipulated with electric and magnetic fields. For fusion to occur without strong pressure the temperature must be very high, typically around 100 million Kelvin for hydrogen [6]. At this temperature fusion reactions become self-sustaining which means that there is enough energy to overcome the electrical repulsion between the protons of hydrogen atoms. In addition to high temperature, the plasma must be confined in a certain region of space during sufficient time for the fusion to occur [6].

Generally, tokamaks are composed of three main electromagnetic systems, ohmic heating system, equilibrium field system, and toroidal field (TF) system [5]. The ohmic heating system

produces the electric field used to break down the plasma, and drives a high plasma current which produces ohmic heating due to the ohmic resistance of the plasma. This system supplies the temperature needed for fusion to occur inside the chamber. The equilibrium field system provides the MF that ensures the radial equilibrium of the plasma. The plasma tends to expand radially due to the higher pressure inside, this force is balanced by the equilibrium field. The TF system provides the toroidal MF that confines the plasma, preventing the plasma column from contacting the chamber wall. This system includes the TF solenoid and the direct current (DC) power supply [5].

Tokamak ISTTOK

The ISTTOK is a relatively small tokamak with a circular cross-section and an iron core transformer [7]. This tokamak operates solely in an inductive way by means of the iron core, and has the same design of the TORTUR, acronym for TORus for TURbulent heating [8].

History and Precedents

The commissioning of the ISTTOK tokamak began officially in January 1990, date when the EUROTOM association agreement was signed [7]. The ISTTOK was assembled from the basic structure of the past experience TORTUR tokamak, conducted by the EURATOM-FOM (Rijnhuizen) association in Niewegein (Netherlands). This includes the support structure, vacuum chamber, copper shell, transformer, toroidal magnetic field coils and capacitor banks, dismantled form the ex-tokamak in 1988. The rest of the components include the vacuum systems and gas supply, power supplies, diagnostics and system control and data acquisition. These parts were developed by other associations. The present toroidal field power supply was awarded from national companies [9].

Technical Data and Features

The technical data and main parameters of the ISTTOK are presented in Table 2.1, regarding the geometric parameters, and Table 2.2, regarding the typical discharge parameters [7, 9].

Table 2.1: Geometric parameters of ISTTOK, adapted from [7].

Geometric Parameters	Value
Larger radius	0.46 m
Minor radius	0.085 m
Maximum toroidal magnetic field	2.8 Tesla
Available flux (primary transformer)	0.25 Vs

ISTTOK is equipped with a tunnable TF, enabling cyclotronic frequency adjustment. This tokamak was the first one equipped with a switchable insulated-gate bipolar transistor (IGBT) primary

Table 2.2: Plasma discharge parameters of ISTTOK, adapted from [7, 9].

Discharge Parameters	Value
Plasma current	$\sim$ 7 kA
Duration of the discharge (DC)	$\sim$ [35,45] ms
Duration of the discharge (AC)	$>$1000 ms
Plasma density @ r=0	$\sim$ 5x10^{18}m^{-3}
Electron temperature @ r=0	$\sim$ 120 eV
Ion temperature @ r=0 (CIII)	$\sim$ 100 eV
Energy confinement time	$\sim$ 0.8 ms
Beta @ r=0	$\sim$ 0.6%
Safety factor	q(0)$\sim$ 1, q(a)$\sim$ 5

circuit allowing multiple alternating current (AC) discharges. ISTTOK is also equipped with a heavy ion beam diagnostic, for temperature and plasma density measurement. The operation of ISTTOK is limited in single pulse mode to around 40 ms of plasma duration, due to core saturation, however, in AC mode this parameter is far greater reaching more than 1 s [8].

Normal Operation Conditions

The tokamak ISTTOK is a pulse power application with a distinctive functioning. The permanent operation regime is characterized by a cycle with a pulse duration of 3 seconds and a rest period (interval between pulses) of approximately 15 minutes. Therefore, the tokamak works in an intermittent regime. The maximum intensity of the current that flows through the TF coils is 8500 A. This limit is imposed by the maximum power demand from the public grid, which is 1 MVA. In addition, the minimum value for this current is 4000 A. This was calculated considering the minimum value for the toroidal magnetic field (MF) of interest to the project, which is 0.3 T [10]. The voltage across the TF coils is less than 100 V.

Toroidal Field System

The TF System includes the coils that produce the toroidal MF, and their power supply which will be analysed in detail in Section 2.3. The toroidal MF has the maximum reach of 2.8 T, this value corresponds to a current intensity of 40 kA. However, due to the power restriction of 1 MVA imposed by the public grid, the toroidal MF density is limited to approximately 0.5 T, which corresponds to a current intensity of 8500 A. The minimum value for the MF that is enough for the project is 0.3 T. The TF is produced by a toroidal solenoid made of 24 coils with water cooling. The data for these coils is presented in Table 2.3 [10].

Since the current that flows through the TF coils can reach values up to 8500 A, the remaining energy stored on this inductor at the end of the tokamak operation, is significant. The energy

Table 2.3: Parameters of the TF coils of the ISTTOK, adapted from [10].

Toroidal Solenoid Parameters	**Value**
Number of coils	24
Maximum current	40 kA
Maximum magnetic field	2.8 T
Electrical resistance	10 mΩ
Inductance	1.88 mH
Time constant	0.188 s

stored in an inductor is proportional to the square of the current, and it is given by

$$E_L = \frac{1}{2} L I^2 \tag{2.1}$$

Where E_L is the magnetic energy stored, L is the inductance value, and I is the current value. The leftover energy is not reused on the tokamak, instead, it is injected back into the public grid of EDP, which is the company that owns it. Ideally, this process should be favourable since the energy is returned, unfortunately in practice, this is not the case. The concern is that the frequency in which the current is re-injected is much smaller than the grid frequency, consequently, this process causes disturbances and quality issues on the public grid.

2.3 Existing Power Supply of ISTTOK

The coils that produce the toroidal MF of the ISTTOK are supplied by a DC power supply. This one megawatt power supply is a 12-pulse assembly based on the parallel association of 4 three-phase thyristors half-wave rectifiers. Due to the power limit of 1 MVA, the maximum intensity of the output current defined is 8500 A. This maximum limit determines that the output voltage shall be lower than 100 V. The power supply is composed by 3 main blocks [10]:

- Measuring and protection equipment;
- Step-down transformers;
- Rectifier with controllable output current.

2.3.1 Connection to the Grid and Power Transformers

The rectifier power supply is connected to the Medium Voltage (10 kV) grid, of EDP. Before the rectification stage, the voltage must be reduced, which is performed by two power transformers. Both transformers have a three-phase double star secondary connection, with opposite phase windings (180 degrees out of phase). For the primary side, one of the transformers is connected in star configuration and the other in delta configuration. As a result, a 30 degrees phase shift is

achieved between the secondary voltages of the two power transformers [10]. With this configuration, it is obtained a twelve-pulse system. The data and parameters of the power transformers are represented in Table 2.4.

Table 2.4: Data and parameters of the power transformers, adapted from [10].

Data	**Transformer Y Y Y**	**Transformer D Y Y**
Manufacture	France Transfo	France Transfo
Type	Dry	Dry
Secundary configuration	3 Phase Double Star	3 Phase Double Star
Sec. Phase Voltage (RMS)	80 V	80 V
Sec. Phase Current (RMS)	1090 A	1090 A
Primary configuration	Star	Delta
Pri. Phase Voltage (RMS)	$10/\sqrt{3}$ kV	10 kV
Pri. Phase Current (RMS)	21.4 A	12.3 A
Short Circuit Impedance	6 %	6 %

2.3.2 Association of Rectifiers

The 12-pulse rectifier converts the AC output of the transformer to DC for the TF coils. Taking into consideration the operation conditions, high current and low voltage, the parallel association of half-wave rectifiers was adopted. The power supply was assembled based on the parallel association of 4 three-phase half-wave rectifiers, with common cathode. This configuration can be divided into one half that is connected to the star transformer, and the other half that is connected to the delta transformer. Furthermore, each half (six-phase systems) can be divided into 2 three-phase rectifiers which are connected to the secondary windings of the transformer (the three-phase rectifiers are in phase opposition). When the AC sources of the rectifiers are out of phase the connection must be performed via an interphase reactor (transformer) [10]. The input terminals of this transformer are connected to the output of each rectifier, and the common point in the middle of the windings, output terminal, is connected to the next stage or the load. This association is represented in Figure 2.1.

This Figure shows the two interphase inductors (L) that connect the three-phase systems, and the interphase inductor (L_1) that connects the six-phase systems. The load (L_{TF}) is the TF coils. In this configuration the voltage drop across the semiconductors is low because of the half-wave rectifiers assembly. Unfortunately, this configuration penalizes the ratio of output power regarding the apparent power of the transformers [10].

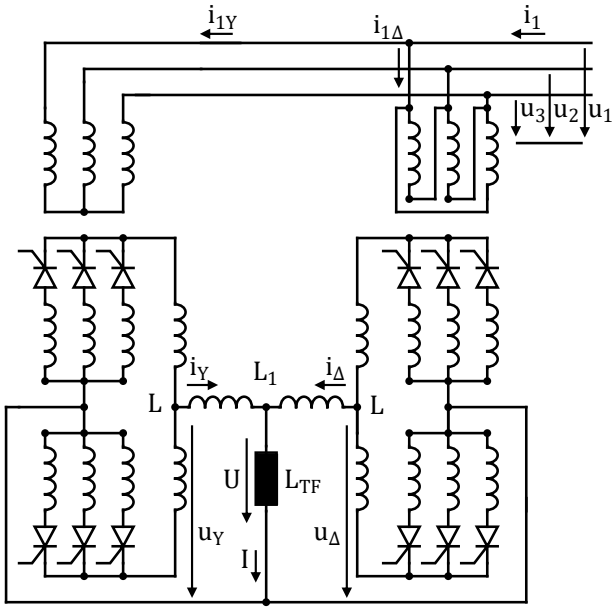

Figure 2.1: Connection scheme of the rectifier, and representation of the different elements of the system.

Analysis of the Output Voltage

Even though the voltage on each input terminal of the interphase reactors have the same average value, the instantaneous value is different. Therefore, there will be a voltage across each reactor, which causes a current to flow through it [11]. This current is affected by the harmonic components present in the voltages applied to the interphase transformer. The current that flows through the interphase reactor $L1$ (Figure 2.1) is determined by the harmonic components of the voltage signals u_Y and u_Δ, with angular frequency 6 times the angular frequency of the grid. The output voltage is characterized by a pulse index of 12 [10]. Its average value is given by

$$U_{0av} = V_M \frac{3}{\pi} \sin\frac{\pi}{3} \cos\epsilon \tag{2.2}$$

Where U_{0av} is the average value of the output voltage, V_M is the amplitude of the electromotive forces induced on the secondary windings of the power transformers, and ϵ the trigger angle of the thyristors. It is also important to refer that the average value of the output voltage of the three-phase, six-phase and twelve-phase systems is the same.

In order to obtain the amplitude of the output voltage, it is possible to consider the parallel association of 4 three-phase half-wave rectifiers equivalent to a twelve-phase half-wave rectifier [10]. As a result, it is established that

$$U_{0M} = V_M \cos\frac{\pi}{6} \cos\frac{\pi}{12} \tag{2.3}$$

Where U_{0M} is the maximum value of the voltage.

2.3.3 Control of the Output Current

The instantaneous value of the output current is approximately equal to the average value, due to the low ripple current. The current in each semiconductor is a fraction of the total output current as a consequence of the parallel association. The value of the current injected into the TF coils must match the reference value selected. In order to regulate the output current, controllable semiconductor rectifiers were selected, in this case, thyristors [10]. Due to the parallel association of rectifiers, the current should be equally divided by the four paralleled fractions. The control of the output current is achieved with feedback loops in each of the 4 three-phase systems. The trigger angle for each group of three thyristors is adjusted based on the current measured in the output of each of these systems.

The instantaneous value of the current is measured by a current transformer and compared with the predefined reference value. The error between these two magnitudes is the input of the compensator which produces the control voltage of the rectifier. The controller must enforce the output current equal to the reference current in steady-state. Thus, the compensator is a proportional-integral (PI) controller and guarantees zero steady-state error [10, 11].

2.4 Energy Storage Technologies

The purpose of energy storage technologies (ESTs) is to store energy in a form that will be later turned into useful energy, hence reusing it whenever needed. The process of capturing energy is the charging stage and the process of releasing energy is the discharging stage [2]. There are different ways to classify ESTs into categories, typically they can be divided according to the form of the converted energy. Thus, energy storage systems (ESSs) may be broadly classified into 5 main categories: thermal, chemical, electrochemical, electrical and mechanical [3].

Thermal ESSs store heat by heating or coaling a thermal medium so that the stored energy can be used for heating or cooling processes. Chemical ESSs store energy in chemical compounds which are used in chemical reactions to release energy. Electrochemical ESSs store energy in chemical form which is then transformed into electrical energy. Batteries and supercapacitors are classified as electrochemical EST. Electrical ESSs are divided into electrostatic and magnetic. The electrostatic category includes some types of capacitors, like electrolytic and film capacitors, and the magnetic includes superconductor magnetic energy storage. Mechanical ESSs are based on the motion and position of an entity. There are two types of mechanical energy, kinetic and potential. A flywheel is classified as a kinetic ESS [3].

In order to evaluate if a given EST is suitable for a specific energy storage application there are some factors that must be taken into consideration. Every EST has specific characteristics that help determine what are the possible applications. The most important features of ESSs are: energy density, power density, storage capacity, storage duration, life time, round trip efficiency,

response time, costs and technological maturity [2, 12].

- Energy density is the quantity of energy stored per unit volume or mass.
- Power density is the amount of power output per unit volume or mass.
- Storage capacity is the total energy stored in the system, different from the retrieved energy.
- Storage duration is related to self-discharging losses and indicates the period of time in which the energy can be retained by the ESS.
- Life time corresponds to the life span of an ESS and the number of charge/discharge cycles.
- Round trip efficiency is the ratio between the energy retrieved from the storage device and the energy put into.
- Response time is how fast an ESS is able to release the stored energy to meet the demand.
- The costs of an ESS include capital and operation costs.
- Technological maturity is how much developed an EST is regarding its industrial application.

Considering the main features of the ESTs previously presented and the technical characteristics presented in Table 2.5, four candidates were selected: flywheels, high power density batteries, supercapacitors and regular capacitors. Each of these ESSs is analysed in this section, more specifically the principle of operation, the main characteristics, the advantages and disadvantages, and the common applications. Lastly, it is evaluated if the application of each EST is suitable for the energy storage system of the ISTTOK.

Table 2.5: Technical characteristics of ESTs, adapted from [2, 3, 12, 13].

Technology	Specific energy (Wh/kg)	Energy density (kWh/m^3)	Specific power (Wh/kg)	Power density (kWh/m^3)	Power Rating
Flywheel	10-100	20-400	400-1500	1000-5000	0-250 kW
Supercapacitor	2.5-15	10-30	500-5000	10,000- $>$50,000	0-300 kW
Capacitor	$<$0.5	0.1-5	10000-50000	$>$100000	0-400 kW
Li-ion battery	60-200	200-750	500-2000	1500-10,000	0-100 kW
NaS battery	100-240	150-300	150-230	120-230	50 kW-8 MW
SMES	0.5-5	0.2-2.5	500-2000	1000-4000	100 kW-10 MW

Technology	Discharge time	Suitable storage duration	Life time (years)	Cycle life	Round trip efficiency (%)
Flywheel	ms - 15 min	s - min	$\sim$15	$>$20,000	85-95
Supercapacitor	ms - 60 min	s -h	$>$15	$>$100,000	90-95
Capacitor	us - s	ms -min	$\sim$5	$<$50000	70-90
Li-ion battery	min - h	min - days	10	1000-10,000	85-95
NaS battery	s - h	s -h	10 - 15	2500	70-90
SMES	ms - 10 s	min - h	$>$20	$>$100,000	90-98

2.4.1 Flywheel Energy Storage

Flywheel energy storage is a form of mechanical energy storage more specifically kinetic energy [12]. This technology is regarded as the main candidate for energy storage in kinetic form. Flywheels are considered to be one of the most cost-effective and reliable EST for high power applications, providing medium energy density but high power density [14], as shown in Table 2.5.

Theoretical Principles of Operation

Inertia flywheels store kinetic energy in a rotating mass such as a spinning cylinder or disk. Theoretically, the energy stored on a spinning flywheel is proportional to the mass and to the square of the rotational speed, and it is given by

$$E_k = \frac{1}{2} I w^2 \tag{2.4}$$

Where E_k is the kinetic energy, I is the moment of inertia and w is the angular velocity [14]. The moment of inertia is given by

$$I = kmr^2 \tag{2.5}$$

Where k is the inertia constant which depends on the type of the spinning mass, m is the mass of the disk or cylinder and r its radius. Based on (2.4) and (2.5) the best way to increase the kinetic energy of a flywheel is to increase its speed [14]. Unfortunately, the centrifugal forces are also proportional to the square of the rotational speed, determined by

$$F_c = mrw^2 \tag{2.6}$$

Where F_c is the rotor centrifugal forces. In order for the flywheel to sustain high speeds, the rotor materials should be able to hold strong centrifugal forces, therefore they must have high tensile strength and low material density [14].

Flywheel energy storage systems (FESSs) need an electric machine in order to convert energy. When kinetic energy is being converted to electricity the machine is acting as a generator, contrarily when electricity is being converted to kinetic energy the machine is acting as a motor, producing torque [12]. Finally, a power electronic converter is needed to control the input and output power, rotational velocity, and frequency of the flywheel system [14]. This converter connects the grid to the electric machine.

Main Characteristics and Applications

FESSs have certain features that set them apart from other ESTs. The most relevant advantages are the long life span (around 20 years), the capability to operate with little maintenance, high cycle life (between tens to hundreds of thousands) [15], high round-trip efficiency (effective

energy conversion), high power density and medium energy density, stability with temperature variations, and low environmental impacts. The main disadvantages are high material costs, safety concerns in case of rotor failure, heat and noise production, centrifugal forces, gyroscopic effect, and low energy storage time making them suitable for quick applications [12]. FESSs are classified based on their rotational speed in low-speed (below 10,000 rpm) and high-speed (above 10,000 rpm). Low-speed flywheels are commonly made of a metal rotor, however, high-speed flywheels are made of a composite rotor, magnetic bearings and a vacuum container [15].

Flywheel EST is a strong candidate for applications that demand a lot of energy in a short period of time. They are cost-effective, reliable and able to sustain frequent charge and discharge cycles [12]. Some examples of functionality are stationary applications like power quality, uninterruptible power supply (UPS), and grid support (voltage adjustment, frequency regulation, quality services). Other applications are intermittent power pulses that exceed the capability of its energy source (pulsed power) and power factor improvement [15].

Application of Flywheel Technology to the ESS for the ISTTOK

In this section, the practical application of flywheel EST to the ESS for the ISTTOK, is analysed. The coils that create the toroidal MF operate with high currents and relatively low voltages [10]. As a consequence, the generator that converts the kinetic energy of the flywheel into electrical energy would have to withstand this intensity of the current. Generators with this capacity have large dimensions and are very expensive, thus not suitable in this case. In order to increase the power density of a flywheel, Toodeji [16] proposes the combination with supercapacitors installed inside the rotation disk. Also, flywheel units have the capability to produce higher voltages, therefore, the installation of transformers is generally required [14].

The operation conditions of the ISTTOK implies that the power supply works with a 3 s pulse and a 15 min rest cycle. This rest period is a long duration for a flywheel without vacuum chamber and magnetic levitation to store energy without too many losses. The best solution to reduce self-discharge losses is to confine the flywheel within a low pressure casing (vacuum container), and to use magnetic (superconducting or permanent) bearings [15]. Considering that low speed flywheels provide a shorter period of energy storage, the one considered for this application should be a fast flywheel. Taking into consideration all the factors discussed, the application of a FESS to this case would be very expensive and not adequate.

2.4.2 Battery Energy Storage

Battery energy storage is classified as electrochemical energy storage. This technology is regarded as the most developed and used. It is the common storage choice for small scale power needs [13]. This section only addresses secondary batteries, these are rechargeable cells. Battery ESSs have relatively high energy densities and voltages [12].

Theoretical Principles of Operation

Batteries store energy in the form of chemical potential, and deliver electrical energy by means of electrochemical reactions [2]. These devices produce direct current (DC). Secondary batteries recharge when a current passes through the circuit in the opposite direction of the normal discharge operation [3]. The charge process is characterized by the increase of chemical potential energy due to the movement of the electrons from the cathode to the anode. Conversely, the discharge process is characterized by the decrease of the stored energy when electrons flow from the anode to the cathode.

Various types of batteries exist including Lead Acid (PbO2), Lithium-ion (Li-ion), Sodium-ion (Na-ion), Nickel Cadmium (NiCd), Sodium Sulphur (NaS), Sodium Nickel Chloride (NaNiCl2), and flow batteries. Aneke and Wang [2] explain these different types of batteries. Generally, the type of battery is labelled based on the materials that compose the electrodes. Currently, lithium cells have gained a major role in ESSs, due to the numerous advantages over other technologies. The most relevant strengths are the high specific energy (per unit weight) and the high energy density (per unit volume) [12], which make them suitable for mobile applications. Among the lithium battery types, Li-ion is the most prominent. These cells use lithium metal or lithium compound for the anode [2]. Li-ion batteries have been summarized in the literature [17]. It is also relevant to mention Sodium-ion batteries. Although the energy and power density of this type of cells is not as high as Li-ion, they are less expensive and there is a high natural abundance of sodium.

A cell is a single unit device and a battery usually consists of an association of cells. Battery ESSs need a battery management system (BMS), which is responsible for equalizing the state of charge (SOC) of all cells. Otherwise, the charge is not distributed uniformly throughout the cells, causing unbalance issues. This process is performed by switch power converters [17].

Main Characteristics and Applications

This section mainly covers Li-ion batteries given that they are the main candidates for high power applications in comparison to other battery types [12]. Lithium-based cells have certain advantages, particularly the fact that lithium has the lowest reduction potential of all elements, providing the highest cell potential, it is also the third lightest element, which allows this type of cells to have high storage capacity and power density [17]. Other advantages of Li-ion batteries include no maintenance required for the sealed cells, wide operating temperature range, rapid charging process, flat discharge curve and extensive design flexibility [13]. The main disadvantages are relatively low cycle life and life span when compared to other ESTs, high cell costs, significant charge and discharge randomness, and the fact that lithium is flammable and reacts with water and moisture [13].

For fixed applications, where the weight is not a relevant factor, lead-acid batteries are a common choice. For mobile applications, Li-ion batteries are the main candidates due to lightweight.

They are mainly used in portable electronics, vehicles, power tools, and electric grid and renewable energy applications [2, 17].

Application of Battery Technology to the ESS for the ISTTOK

In this section, the practical application of battery EST to the ESS for the ISTTOK, is analysed. The tokamak operation is characterized by high-power pulses. Batteries are not the most appropriate technology for this purpose. Flywheels and supercapacitors ESSs are able to withstand higher power, making them more suitable for pulse applications. The power density of batteries makes this technology not appropriate for this operation. On the other hand, the energy density is excessive, therefore, a lot of the storage capacity would be wasted. The number of cycles is also a drawback, the life span of batteries is not as high as the other technologies presented. Considering these factors, the application of batteries is not adequate.

2.4.3 Supercapacitor Energy Storage

Supercapacitor energy storage is classified as electrochemical energy storage. This technology has been developing rapidly and shows promise. In comparison to conventional capacitors, the storage capacity is much higher, however, supercapacitor cells have low voltage levels. Above all, these devices manage high power output in short periods of time [13], as shown in Table 2.5.

Theoretical Principles of Operation

Supercapacitors are also known as ultra-capacitors or electrochemical capacitors. They are classified into the same category as batteries (electrochemical storage), and differ from the electrolytic capacitors and electrostatic capacitor, which have lower capacitance values [2]. The energy stored in a capacitor is given by

$$E_C = \frac{1}{2}CV^2 \tag{2.7}$$

Where E_C is the energy stored, C is the capacitance value and V the electric potential difference. In addition, the variation of energy in a capacitor is given by

$$\Delta E = \frac{1}{2}C(V_f^2 - V_i^2) \tag{2.8}$$

Where ΔE is the variation of energy stored, V_f is the final voltage and V_i is the initial voltage. There are three leading types of supercapacitors including pseudocapacitors, electrochemical double-layer capacitors and hybrid capacitors [15]. This section focus on the double layer type. Supercapacitor cells comprise an electrolyte, two electrodes and a separator. They store electricity by means of ions on an electrolyte solution between solid conductors. The ions are assembled close to the surface of highly porous materials with a very large surface area. When voltage is

applied to the terminals, the electrodes are polarized causing the ions in the electrolyte to form double-layers of opposite charge to the electrolyte [2, 13]. Recently, research in this energy storage technology has been abundant, like the application of nanoscale research [12].

Main Characteristics and Applications

The main advantages of supercapacitor ESSs are the high round trip efficiency (up to 95%), the fast response time, they can respond to changes in power demand in milliseconds, the very high cycle life, these cells can be cycled hundreds of thousands of times without losing storage capacity [12]. These devices have the highest power density of all ESTs reviewed until now [2, 12], being capable of supplying high peak power output. Other strengths are the fast charging time and low impedance. On the other hand, the main disadvantage is the low energy density which highly conditions their application, currently supercapacitor cells store much less energy than batteries (1-2 orders of magnitude) [12]. Other drawbacks are the low cell voltage (many serial connections are required to obtain high voltage), and their susceptibility to self-discharge.

This EST is less common when compared with the others that were reviewed, regardless, some applications are regenerative braking systems, for example in vehicles and electric rail transit systems [15], renewable energy systems, UPS, peak demand reduction, dynamic voltage restorer for dips, voltage and frequency regulation [12].

Application of Supercapacitor Technology to the ESS for the ISTTOK

In this section, the practical application of supercapacitor EST to the ESS for the ISTTOK, is analysed. The tokamak operates with high currents and relatively low voltages ($<$ 100 V), these conditions validate the application of supercapacitors. This EST is capable of high power output in short periods of time which is appropriate for pulsed applications like the tokamak. The major issue is the short amount of energy that supercapacitors are able to store when compared with the other storage technologies, nevertheless the energy requirement for this application is not excessive. Another pertinent concern is the discharge curve of the capacitors, which is not flat. This means that the voltage does not remain constant as the energy is used up. From 2.7 the energy on the supercapacitor cells is proportional to the square of the voltage, this might be inconvenient when designing the capacitor bank. Considering all of the factors presented, this candidate appears to be the most promising.

Available Products on the Market

To conclude the research on this EST an analysis of the products currently available was carried out. Table 2.6 shows different supercapacitor cells and their parameters. These ratings were extracted from the datasheets of the components.

Table 2.6: Parameters of the supercapacitor cells extracted from the datasheets.

Cell ref.	Brand	Cc (F)	Vr (V)	ESRc (mΩ)	AMCc (A)	AMVc (V)	Isc (A)
SCA0300	Skelcap	300	2.85	1.60	300	3.00	3000
SCA3200	Skelcap	3200	2.85	0.18	3100	3.00	20400
BCAP0350	Maxwell	350	2.70	3.20	170	2.85	840
BCAP3000	Maxwell	3000	2.70	0.29	1900	2.85	9300
LSUC3000	LS Mtron	3000	2.80	0.36	2019	3.00	7700

The parameter Cc is the capacitance per cell, Vr is the voltage rating, ERCc is the equivalent series resistance of the cell, AMCc the absolute maximum current, AMVc the absolute maximum voltage which can be also refer to has the surge voltage (Vs), and Isc the short circuit current.

2.4.4 Electrolytic Capacitor Energy Storage

Electrolytic capacitors store the electric energy statically. In comparison to supercapacitors the capacitance is much smaller, however, electrolytic capacitors are capable of charging and discharging in milliseconds. Of all the storage technologies presented in this chapter this one has the highest power density and lowest energy density (Table 2.5).

Theoretical Principles of Operation

An electrolytic capacitor is a polarized capacitor that uses an electrolyte as the negative plate or cathode to achieve a larger capacitance value than other types. The positive plate or anode is a metal foil covered with an insulating oxide layer. This layer is the dielectric of the capacitor which separates the two electrodes and it is form through anodizing [18]. There are three types of electrolytic capacitors: tantalum, niobium and aluminium. The most common is aluminium, the cells that will be presented belong to this type. When voltage is applied to the terminals, electrical energy is converted into electrostatic charge, as a result the capacitor charges. The process is reversed during the discharge. The energy stored is given by (2.7) and its variation by (2.8).

Main Characteristics and Applications

The main advantages of the electrolytic capacitors are the high voltage rating capability, much higher than supercapacitors, the high surge current and the very fast response time, allowing the capacitor to fully charge and discharge in very short periods (order of milliseconds). The principal disadvantage is the very low energy density when compared to the other ESTs that were presented. Other drawbacks are the large leakage currents, the risk of explosion, and the short lifetime when the capacitor is not used, due to the decrease of the dielectric on the anode foil [19].

Regarding the main applications, some examples are frequency filters like high pass, low pass and noise filtering, coupling and decoupling of signals and avoiding excessive drawing of power.

Other uses are reactive power control, power factor correction and smoothing of output voltage in power supplies [19].

Application of Electrolytic Capacitors to the ESS of the ISTTOK

In this section, the practical application of electrolytic capacitors to the ESS of the ISTTOK, is analysed. Due to the very low energy density of these capacitors the only possible application on the TF system is to store the energy left in the coils at the end of the pulse. Since this type of cells are able to charge and discharge very quickly, the energy transfer between the coils and the electrolytic capacitors can be very fast, insuring few losses during this process. Although the energy density is small, the power density is the highest of all ESTs. Finally, like the supercapacitors, the discharge curve of these cells is not flat.

Available Products on the Market

An analysis of the electrolytic capacitor cells currently available on the market was carried out, resulting in Table 2.8 which shows their parameters. These ratings were extracted from the datasheets of the components. All the parameters presented in this table have the same names as the ones presented in Table 2.6, thus, they were already explained.

Table 2.7: Parameters of the electrolytic capacitor cells extracted from the datasheets.

Cell reference	Brand	Cc (uF)	Vr (V)	Vs (V)	ESRc (mΩ)	Isc (kA)
DCMC153T400FG2D	CDE	15000	400	450	13.1	30.5
DCMC383T250FG2D	CDE	38000	250	300	9.2	27.2
E37X501CPN103MFM9U	Chemi-Con	10000	500	550	12	41.7
E37X401CPN153MFM9U	Chemi-Con	15000	400	450	7	57.1
B437*7A9159M6##	TDK	15000	400	450	14	28.6

2.5 Semiconductor Devices

Generally solid-state materials are divided into three classes: conductors, insulators and semiconductors. The electrical conductivity value of a semiconductor is between the value of a conductor and an insulator. The conducting properties of these materials can be controlled by external and internal factors, like electric and magnetic fields [20]. Semiconductor devices are a type of electronic components that relies on this ability to manipulate the conductivity [21]. There are many types of semiconductor devices, however, this section only covers the ones that are more relevant for this project which are: Power Diodes, IGBTs and Thyristors.

Diodes are devices with 2 terminals having PN or PN-N+ junctions. They are unidirectional (positive current capability, negative voltage blocking state) and uncontrollable, which means that

the operation state is entirely determined by the external circuit. A diode is forward biased during conduction, and reversed biased when it is blocking [22].

Insulated Gate Bipolar Transistors (IGBTs) are devices with 3 terminals, unidirectional and fully-controllable, which means that it is possible to set the operation mode between conduction and blocking using the gate. This type of device combines high efficiency and fast switching. IGBTs have high input impedance and low saturation voltage, as a result, they are able to withstand a large collector-emitter current with almost zero gate current drive [22].

Thyristors, also known as Silicon Controlled Rectifiers (SCRs), are devices with 3 terminals and usually 4 layers. They are unidirectional and semi-controllable, which means that they can be turned on but cannot be turned off directly from the gate. This type of device has a very high peak pulsed current capability, and is capable of handling large variations of current. Thyristors are the selected semiconductor switches for electromagnetic launchers (also known as railguns), which is an application that requires the switching of high pulse currents in very short intervals [23].

Available Products on the Market

Considering the high intensity of current that the TF coils operate with, the selected semiconductor devices must be significantly large and powerful. Table 2.8 was built after an analysis of the products currently available on the market. This table shows a few semiconductor devices and their parameters. These ratings were extracted from the datasheets of the components.

Table 2.8: Parameters of the semiconductor devices extracted from the datasheets.

Product ref.	Brand	Device Type	Ir (A)	Is (kA)	Vr (V)	Ron (mΩ)	Vf (V)
FZ3600R17HP4	Infineon	IGBT	3600	7.2 (1 ms)	1700	0.30	0.7
FZ2400R17HP4	Infineon	IGBT	2400	4.8 (1 ms)	1700	0.45	0.7
DZ3600S17K3	Infineon	Diode	3600	7.2 (1 ms)	1700	0.19	0.7
DD1200S17H4	Infineon	Diode	1200	2.4 (1 ms)	1700	0.63	0.7
KP720LT	YZPST	Thyristor	3500	60 (10 ms)	1400	0.076	0.86
KP800A	Huajing	Thyristor	800	10 (10 ms)	1200	0.42	0.85

Product ref.	td-on (us)	td-off (us)	tr (us)	tf (us)	Eon (mJ)	Eoff (mJ)
FZ3600R17HP4	0.55	1.60	0.28	0.21	780	1200
FZ2400R17HP4	0.65	1.30	0.20	0.19	405	660
DZ3600S17K3	10.0	-	-	-	-	575
DD1200S17H4	10.0	-	-	-	-	180
KP720LT	-	15	-	-	-	-
KP800A	-	400	-	-	-	-

The parameter Ir is the current rating, Is the surge current with the associated maximum time,

Vr the voltage rating, Ron the internal resistance of the component (on state), Vf the forward voltage, td-on the turn on delay time, td-off the turn off delay time, tr the rise time, tf the fall time, Eon the turn on energy loss per commutation, and Eoff the turn off energy loss.

2.6 Resonant Circuits (series RLC)

An electric circuit including an inductor and a capacitor may operate as a resonant circuit (LC circuit). If the circuit also includes a resistor it becomes an RLC circuit where the components can be connected in series or in parallel. The RLC circuit resonates in a similar way as the LC circuit, except with the resistor there is damping [24]. The majority of the circuits that will be covered in the next chapters operate with an inductor (TF coils) and a capacitor bank in series. Figure 2.2 shows an example of an RLC circuit with the initial conditions describing the end of the pulse.

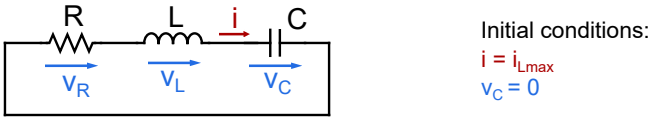

Figure 2.2: RLC circuit schematic with initial conditions set.

The constitutive equations that describe the behavior of the components of an RLC circuit are

$$\begin{cases} v_R = Ri(t) \\ v_L = L\frac{di(t)}{dt} \\ v_C = v(0) + \frac{1}{C}\int_0^t i(\tau)\,d\tau \end{cases} \tag{2.9}$$

Where v_R is the voltage across the resistor, v_L the voltage across the inductor and v_C the voltage across the capacitor. First, the Kirchhoff's voltage law is applied to the series RLC circuit. The governing differential equation of the circuit is obtained by replacing the terms of the equation obtained from the Kirchhoff's voltage law by the constitutive equation of each component [25]:

$$Ri(t) + L\frac{di(t)}{dt} + v(0) + \frac{1}{C}\int_0^t i(\tau)\,d\tau = 0 \tag{2.10}$$

Afterwards, taking the time derivative and dividing the terms by the inductance L results in the following second order differential equation

$$\frac{d^2i}{dt^2} + \frac{R}{L}\frac{di}{dt} + \frac{1}{LC}i(t) = 0 \tag{2.11}$$

This equation can also be expressed as

$$\frac{d^2i}{dt^2} + 2\alpha\frac{di}{dt} + \omega_0^2 i(t) = 0 \tag{2.12}$$

Where α is the damping attenuation and ω_0 is the resonance angular frequency. The damping attenuation and resonance frequency are respectively given by

$$\alpha = \frac{R}{2L} \tag{2.13}$$

$$f_0 = \frac{\omega_0}{2\pi} = \frac{1}{2\pi}\frac{1}{\sqrt{LC}} \tag{2.14}$$

Even though the circuits that will be analysed have some resistance (due to the internal resistance of the components) its value is very low in relation to the other parameters, therefore they can be analysed considering an LC circuit. The solution of (2.11) is obtained through the use of Laplace transforms. Considering that the circuit is an LC circuit (the parameter R is null), the solution of (2.11) is given by

$$i(t) = I_0 \cos(\omega_0 t + \phi) \tag{2.15}$$

Where I_0 is the maximum amplitude of the current, and ϕ the phase of the signal. The voltage across the capacitor is the symmetrical of the voltage across the inductor and it is given by

$$v_C(t) = -L\frac{di(t)}{dt} = L\omega_0 I_0 \sin(\omega_0 t + \phi) \tag{2.16}$$

At the end of the pulse the TF coils are fully charged and the capacitor bank discharge, consequently, the initial conditions of the circuit are characterized by the maximum current (I_0) through the inductor and null voltage across the capacitor. As a result, the phase (ϕ) is zero. By examining (2.15) and (2.16), it is possible to verify that the current and the voltage waves are 90 degrees out of phase. This means that the energy transfer between the inductor and the capacitor takes a quarter of the period of resonance, simply put

$$t_d = \frac{1}{4f_0} = \frac{\pi\sqrt{LC}}{2} \tag{2.17}$$

Where t_d is the discharge time (how long it takes for the energy to be transferred).

3

Current Power Supply of the Toroidal Field Coils

Contents

3.1 Introduction

Before the design of the energy storage system, it is essential to analyse the existing power supply of the TF coils in use. This chapter covers the results obtained for the existing energy source, which is a twelve-phase assembly based on the parallel association of 4 three-phase half-wave rectifiers. This power supply was simulated using MATLAB and Simulink. The implementation is divided into 4 parts: the power transformers, the rectifier, the thyristors trigger system and the PI control. The most relevant results and simulations are presented and analysed.

3.2 Power Transformers

The connection of the power supply to the public grid is performed via two power transformers.

3.2.1 Implementation of the Power Transformers

Each three-phase transformer was implemented using three single-phase linear transformers, each with three windings, one primary and two secondaries. The connection scheme is presented in Figure 3.1. The left assembly constitutes the transformer with the primary windings connected in star and the right assembly constitutes the transformer with the primary windings connected in delta. Both transformers have the secondary windings connected in a way to obtain a three-phase double star connection, with opposite phases. The parameters used for the models of the power transformers are represented in Table 2.4.

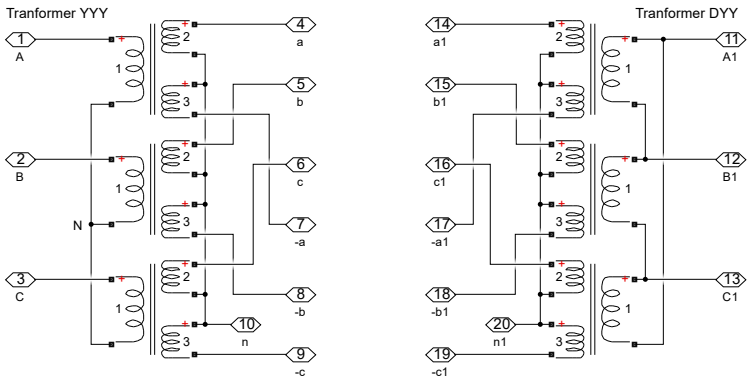

Figure 3.1: Simulink implementation of the power transformers and connections.

3.2.2 Current Demanded from the Public Grid

Figure 3.2 represents the current demanded from the public grid in steady-state for an output pulse of 7000 A. This current is equal to the sum of both currents on the primaries of the transformers. Figure 3.2 (a) represents the results obtained by simulation for the currents on the three phases and Figure 3.2 (b) represents the experimental results for the current on a single phase.

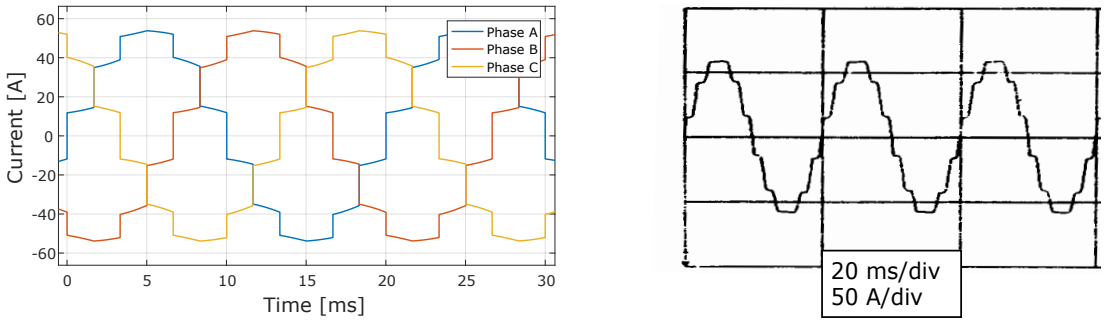

Figure 3.2: Current demanded from the grid in steady-state for a pulse of 7000 A: (a) Simulink simulation; (b) Real system, adapted from [10].

3.3 Twelve-Pulse Rectifier

The connection of the power transformers to the toroidal field coils of the tokamak is performed using a parallel association of 4 three-phase half-wave rectifiers with interphase reactors but no output capacitive filtering.

3.3.1 Implementation of the Twelve-Pulse Rectifier

This association was already covered in Section 2.3. The implementation of the rectifier is represented in Figure 3.3. The system can be divided into two six-phase associations, the left connected to the YYY transformer (star configuration) and the right connected to the DYY transformer (delta configuration). It is important to note that the numeric order of thyristors for each six-phase association, corresponds to the natural order of commutation of a three-phase thyristor bridge rectifier. As a result, the first three-phase system comprises the thyristors T1, T3 and T5.

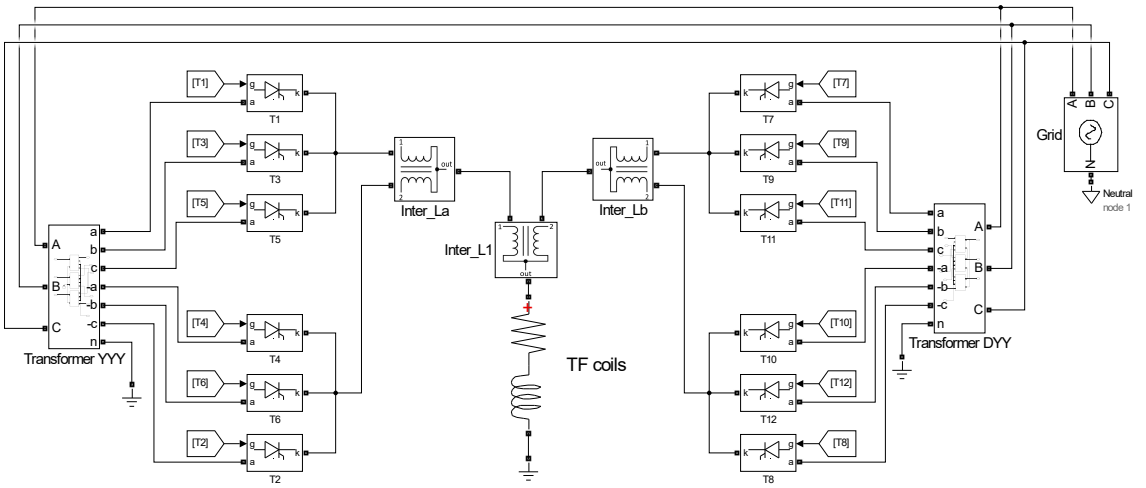

Figure 3.3: Implementation of the power section of the rectifier circuit.

Each interphase reactor is implemented with three ideal inductors. The corresponding equivalent circuit is composed of two inductances with value L1 and L2 and a negative series inductance

(–M) connected to the middle point, as represented in Figure 3.4 (a). L1 and L2 are the self inductances and usually they are identical to each other, thus the value of the inductance is the same for both of them. M is the mutual inductance and typically its value corresponds to half of the self inductance. Figure 3.4 (b) represents the implementation of one interphase transformer in Simulink. The design of interphase reactors is further elaborated in the literature [26, 27].

Figure 3.4: Interphase reactors: (a) equivalent circuit; (b) implemented circuit.

The inductances of the interphase transformers were computed using two different methods. The results obtained using both procedures were very similar. The first one is described in the literature [10] and the second one is based on the Fourier series of the output voltage. The resulting equation that express the value of the inductance is given by

$$L > \frac{2U_{0av\_max}\sqrt{(kp)^2 sin^2(\epsilon) + cos^2(\epsilon)}}{\omega kp I_{L\_min}((kp)^2 - 1)} \tag{3.1}$$

Where L is the required inductance, U_{0av_max} the maximum average output voltage, ϵ the trigger angle, ω the angular frequency and k an integer that assures that the output voltage harmonics are multiples of the pulse index (p). Finally, I_{Lav_min} is the minimum average current, this value must assure the operation in continuous conduction mode (CCM), for that matter it must be higher than half of the current variation (ripple). The value of the inductance must be computed considering the worst case scenario. This corresponds to a trigger angle of 90 degrees which leads to the maximum value of inductance. The maximum average output voltage is computed using (2.2). The value of the term kp is 3 for the interphase reactors that connect the three-phase rectifiers, and 6 for the interphase reactor that connects the six-phase systems.

3.3.2 Voltage and Current Analysis in Different Stages of the Rectifier

It is essential to analyse the voltage and current values in different points of the circuit. The simulation of the steady-state voltage at the output of 5 crucial stages of the rectifier is represented in Figure 3.5, for a trigger angle of 45 degrees. The signals u1 and u2 are the output voltages of the first three-phase rectifier (T1, T3 and T5), and the second three-phase rectifier (T4, T6 and T2), respectively. The signals uY and uD are the output voltages of the two six-phase systems, and Uo is the output voltage of the whole system. Figure 3.5 also shows that the mean output voltage value is the same for all these systems.

The simulation of the steady-state current that flows through the interphase reactors is represented in Figure 3.6, for an output current of 6000 A. Figure 3.6 (a) represents the currents that

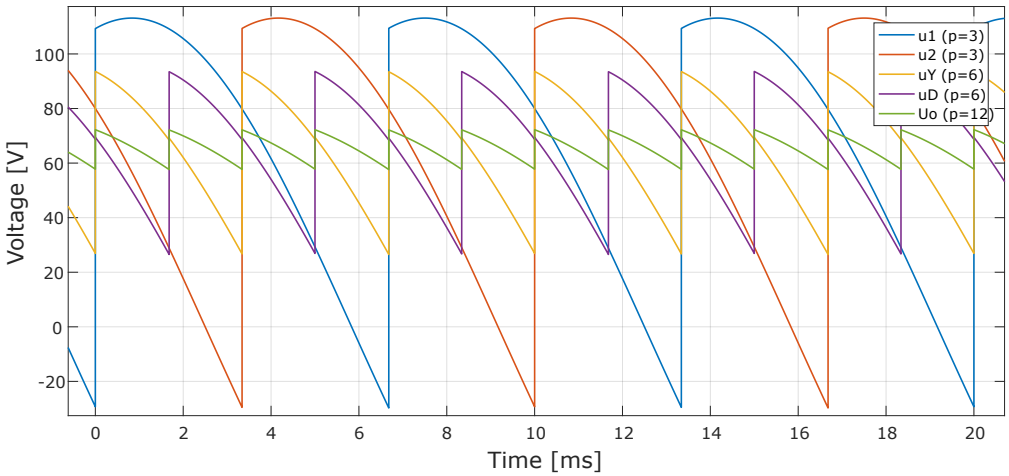

Figure 3.5: Steady-state voltages at different points of the rectifier for a 45° trigger angle. Waveforms and corresponding pulse index (p).

flow into each input terminal of one of the two interphase transformers that connect two three-phase rectifiers. Figure 3.6 (b) represents the currents that flow into the interphase transformer that connects the two six-phase systems. The current ripple factor is much lower on this second inductor. The output current that enters the TF coils has an even lower ripple and it is represented in Figure 3.6 (c). This current is roughly constant, which demonstrates that the rectifier is capable of providing nearly a DC output, as it is intended.

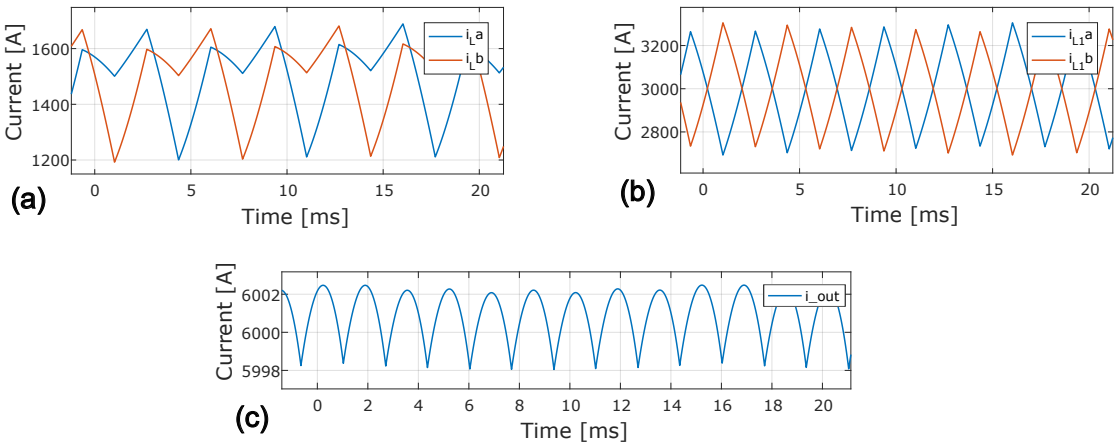

Figure 3.6: Steady-state current: (a) interphase reactor that connects two three-phase systems; (b) interphase reactor that connect the six-phase systems; (c) output of the rectifier.

3.4 Trigger System of the Thyristors

The ON and OFF state of the thyristors is controlled with the trigger system. This system receives as input the trigger angle and outputs the control signal for each thyristor.

Implementation of the Trigger System and Waveforms

Each thyristor has its own control signal which is a pulse wave responsible for the switching. The rectifier has 12 thyristors, therefore the trigger system has to generate 12 control signals. The trigger angle for each group of 3 thyristors is adjusted based on the current measured in the output of each three-phase rectifier. There are 4 three-phase rectifiers connected in parallel, as a result, the trigger system is constituted by 4 blocks that control each group of 3 thyristors. The block that controls the first three-phase rectifier is represented in Figure 3.7.

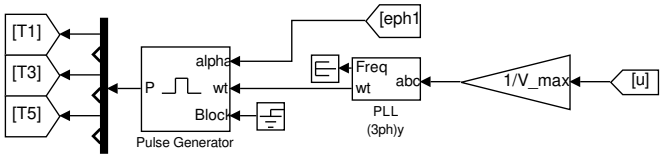

Figure 3.7: Implementation of the trigger system for T1, T3 and T5. This system supplies the control signals to the semiconductor switches.

The input eph1 is the trigger angle (in degrees) for the thyristors T1, T3, and T5. The input u is a three-element vector with the phase voltages of the public grid, which is then normalized. The Phase-Locked Loop (PLL) block generates the saw-tooth carrier waveform which is synchronized with the grid voltage. The Pulse Generator block generates the vector that contains the control signals. These waveforms are represented in Figure 3.8 which shows the operation of the trigger system for a trigger angle of 45 degrees.

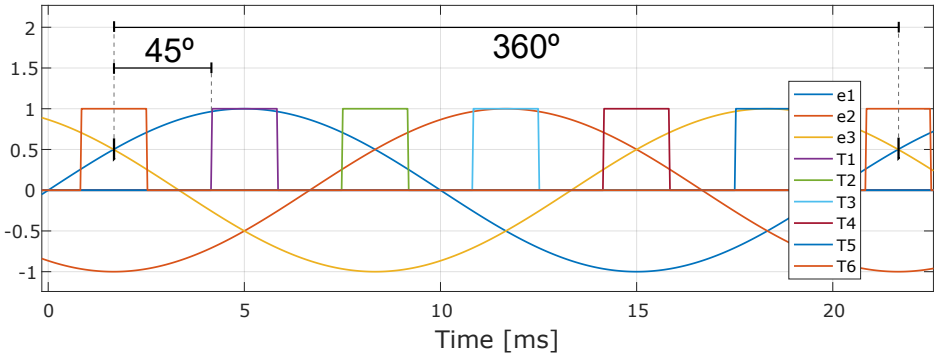

Figure 3.8: Trigger pulse signals for a trigger angle of 45 degrees. Coordination between the waveforms.

The signals e1, e2 and e3 are the normalized phase voltages (vector u), and the other six waveforms are the control signals for each thyristor of the six-phase rectifier connected to the star (YYY) power transformer. Is possible to measure from Figure 3.8 the value of the trigger angle, which corresponds to the time interval between the interception of the signals e1 and e3, and the control signal of the first thyristor (T1). In this case, 2.5 ms corresponds to 45 degrees.

3.5 Proportional Integral (PI) Controllers

The control of the output current is achieved with PI control of the 4 three-phase systems. The TF coils are an extremely inductive load with little resistance, consequently, it is expected a pole at the origin. This factor establishes the control model to be adapted which is represented in Figure 3.9. Each block corresponds to the transfer function of a component. The blue block is the PI compensator, the green block is the rectifier, and the yellow block the inductive load (TF coils).

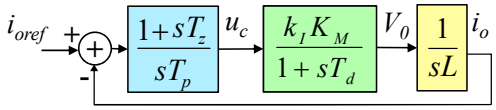

Figure 3.9: Control model for the output current and transfer function of each block (element).

Starting with the rectifier, T_d is the mean delay which corresponds to 20/6 ms considering a pulse index of 3. K_M is the static gain of the converter which is computed based on the maximum control voltage, and the maximum average output voltage. Lastly, k_I is the current gain. For the compensator, the values for T_p and T_z are selected to fastening the transient response and increase the phase margin and bandwidth [28]. The proportional gain (K_p) and integral gain (K_i) are computed based on the values of these time constants. By increasing the proportional gain the system becomes faster but might become unstable. By increasing the integral gain the steady-state error and oscillations decrease but the overshoot increases. The results were obtained based on the content presented in the literature [11]. They are shown in Table 3.1.

Table 3.1: Results obtained for the parameters of the PI controller of the output current.

Parameter	Value
ξ	0.7071
a	2.4142
u_{cmax}	6.2832
T_d	0.0033

Parameter	Value
K_M	-14.780
K_p	-0.0053
K_i	-0.2712
K_W	189.80

3.5.1 Implementation of the PI Controllers

The PI controllers must impose the output current equal to the reference current. This is achieved with a feedback loop for each three-phase rectifier. This implies that the current must be measured at the output of each three-phase system, and the reference current must be a quarter of the output desired current. Another option would be to use only one PI controller and measure the output current of the converter (the whole system) instead. This alternative was not selected due to the unbalance of the currents that flow through the different branches of the circuit, or the interphase reactors. Naturally, all the components have small deviations that cause asymmetries in the system, therefore, to obtain a balance system it is necessary to control each current that

enters the interphase transformers. The circuit that controls the current for each three-phase rectifier is represented in Figure 3.10. The first input (I_ref) is the current reference, which is a quarter of the desired output current, and the second input (i) is the current measured at the output of the three-phase rectifier. The output (eph) is the trigger angle for a single group of 3 thyristors. The PI compensator with saturation comprises the elements inside the blue rectangle. The gain blocks that follow the compensator convert the control voltage value (output of the compensator) to the trigger angle value in degrees.

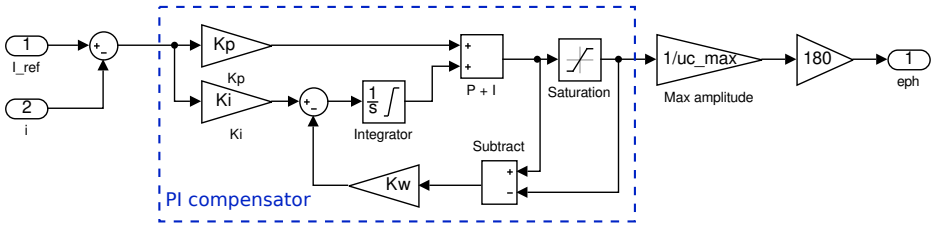

Figure 3.10: Simulink implementation of the PI controller for each three-phase rectifier.

3.5.2 Analysis of the Results for the Current Control

The PI compensator is not able to enforce the control objective (output current equal to reference current) instantaneously. The time evolution of the output current is shown in Figure 3.11, for a desired current of 6000 A. It is possible to compare the results obtained from simulation 3.11 (a) with the experimental results of the real system 3.11 (b). The scale for both figures is the same: 500 ms per division on the x-axis, and 2000 A per division on the y-axis. The time evolution of the output voltage is also presented for the same conditions in Figure 3.12. The y-axis for this figure corresponds to 40 V per division.

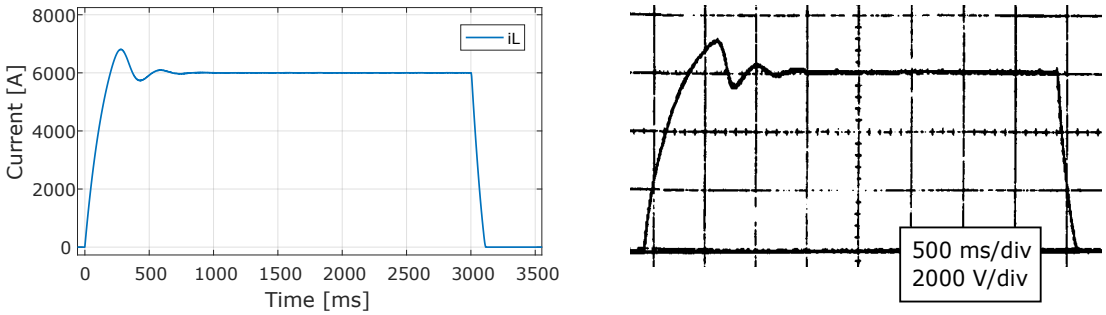

Figure 3.11: Evolution of the output current for a reference of 6 kA: (a) Simulink simulation; (b) real system, adapted from [10]. Initial transient response of the system.

Figure 3.11 also shows the cancellation of the current flowing through the coils. It takes a few milliseconds for the current value to reach zero, during this period the energy left in the coils is re-injected into the grid. This behavior can be confirmed by analysing the voltage across the TF coils at the end of the pulse. Figure 3.12 shows a negative voltage at the terminals of the coils during the cancellation of the current. Since the current is positive and the voltage negative, it means

that the TF coils are supplying energy to the AC network (grid of EDP). The voltage waveform at the steady part of the pulse is similar to Figure 3.5.

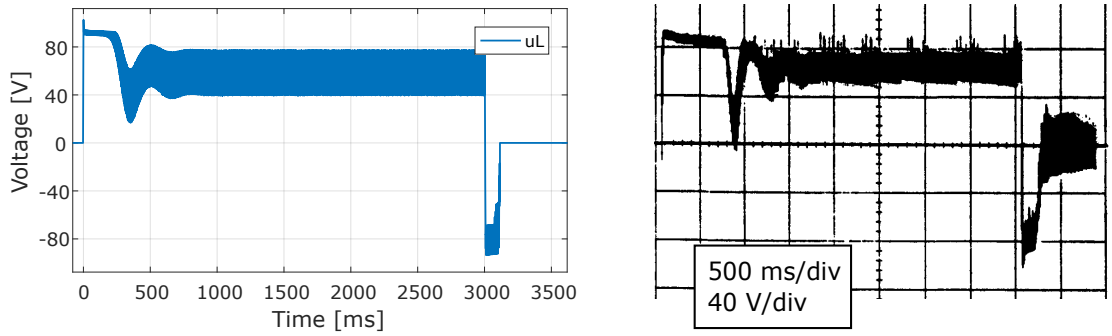

Figure 3.12: Evolution of the output voltage for a reference of 6 kA: (a) Simulink simulation; (b) real system, adapted from [10]. And voltage polarity reversal.

The trigger angle for each group of 3 thyristors during the steady section of the pulse is represented in Figure 3.13 (a), for a desired current of 6000 A. This signal has the same shape as the currents that flow into the interphase reactors that connect the three-phase rectifiers. This is expected since the current is measured at that point, therefore the variation of the trigger angle is caused by the current ripple. The time-evolution of the trigger angle is represented in Figure 3.13 (b). There is a trade between the variation of the trigger angle and the time it takes to reach a steady pulse. In normal operation conditions, by increasing the response of the control system the steady-state will be achieved quicker but the trigger angle variation will increase. It is also possible to use the mean value of each trigger angle signal instead to reduce this variation. Finally the cancellation of the current is achieved by setting each trigger angle of the thyristors to 150°, this can be verified in Figure 3.13 (b).

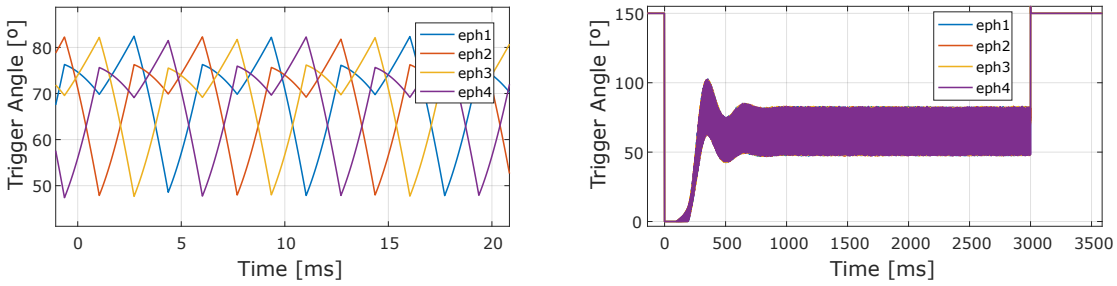

Figure 3.13: Trigger angles for a reference of 6 kA: (a) in steady-state; (b) time-evolution.

4

Design of an Energy Storage System for the ISTTOK

Contents

4.1 Introduction

This chapter covers the different options that were developed and analysed for the energy storage system (ESS). Although they serve similar purposes each alternative has its own functionality and advantages. There are 3 main solutions which are presented in separate sections of this chapter: supercapacitor power supply with additional DC source, modified rectifier power supply with auxiliary capacitor banks, and energy recover upgrade of the existing power supply. In each section the idea and concepts of the solution is explained, along with the computations and the results including the simulation of the circuits. In addition, small variations of the main circuit are considered to enhance different aspects giving diversity to each option. In summary, a description of three distinct ESSs is conducted based on the concepts and content presented in Chapter 2 and Chapter 3.

4.2 Energy Dissipated and Stored in the Toroidal Field Coils

This section presents the initial considerations in order to design an ESS for the TF coils (load). Starting with the power dissipation in the coils during the pulse this is the power of the pulse and the power requirement for the source. This value is obtained with Joule's law and it is given by

$$P_p = R_L I_p^2 \tag{4.1}$$

Where P_p is the dissipated power, I_p is the current intensity of the pulse and R_L the TF coils resistance. Although the resistance of the coils is small (10 mΩ according to Table 2.3) the value of the current during the pulse is very high (kiloamperes) which leads to a high power dissipation. The energy dissipated in the coils is the energy that the power supply needs to provide. This value is obtain by multiplying the power dissipation by the operation time, and established by

$$E_p = P_p t_p \tag{4.2}$$

Where E_p is the dissipated energy and t_p the pulse duration. The load (coils) is extremely inductive, therefore, it is necessary to compute the magnetic energy stored in the TF coils at the end of the pulse. After the operation of the tokamak, the cancellation of the current flowing through the coils is done by inverting the polarity of the voltage of the thyristor rectifier. The value of the magnetic energy stored is calculated from (2.1). Considering the parameters of the TF coils represented in Table 2.3, the results obtained for a few pulses are presented in Table 4.1.

For a pulse with a duration of 3 s the magnetic energy left at the end corresponds to approximately 3 % of the total dissipated energy in the coils, however, its value is still significant since this energy is re-injected into the public grid. The percentage of magnetic energy becomes greater when the duration of the pulse is smaller, as the dissipated energy becomes smaller.

Table 4.1: Power dissipation, energy dissipated and magnetic energy in the toridal field coils.

Current	Power dissipation	Energy dissipated (3 s pulse)	Magnetic energy stored
4000 A	160 kW	480 kJ	15 kJ
6000 A	360 kW	1080 kJ	34 kJ
8500 A	723 kW	2168 kJ	68 kJ

4.3 Supercapacitor Power Supply with Additional DC Source (1st Solution)

In this section, the possibility of replacing the existent power supply with a supercapacitor based power supply is assessed. This solution has the potential to increase the current pulse duration and intensity, to obtain better current rise and fall times, and to recover part of the magnetic energy. The capacitor bank (CB) is charged during the interval between pulses and discharged during the pulse which only lasts a few seconds. The energy stored in the CB must be enough to withstand a current pulse with a specific current intensity and duration. In this solution, the storage system may use another power supply to charge the CB. This DC source can be much smaller and does not need to provide high current, since its function is to only charge the supercapacitors during the period between pulses, which takes a few minutes. By replacing the existing rectifier power supply with a smaller source, which is exclusively responsible for restoring the voltage on the supercapacitor bank, it is possible to reduce the contracted power tariff.

4.3.1 Optimal Sizing of the Supercapacitor Bank

In order to design a supercapacitor power supply, it is crucial to size the optimal capacitor bank (CB) by minimizing the number of cells needed. The CB is formed by associating capacitor cells (CCs) in series and parallel, thus many combinations are possible. The best association is determined by 3 factors: desired current intensity, duration of the pulse, and the selected CC. It is important to note that the configuration that minimizes the number of cells, calculated based on these factors, is only optimal for the particular situation used to determine it, which means that changing the value of any of these 3 parameters will result in a different optimal association. The calculations will be conducted considering 3 different situations for the desired current pulse: 8500 A for 3 s, 15000 A for 3 s and 6000 A for 10 s. The parameters of the supercapacitor cells are presented in Table 2.6.

Minimum and Maximum Voltage of the Supercapacitor Bank

The first step to size the capacitor bank is to determine the minimum and maximum operating voltage which maximizes the useful energy and meets the power demand. Starting with the minimum acceptable voltage, that the CB might reach during the pulse, this value depends on the

desired current intensity of the pulse and the resistance of the TF coils. Since there is no boost converter in this system (to increase the voltage) the minimum voltage must be enough to sustain the desired current through the coils. Therefore, the voltage of the CB must be always greater than the voltage drop across the coils caused by the desired current flowing trough these coils (due to its resistance). In addition the internal resistance of the CB also affects the minimum voltage, due to the voltage drop across the cells. The minimum acceptable voltage (V_{min}) is determined using Ohm's law and given by

$$V_{min} = I_p(R_L + R_{bank}) \tag{4.3}$$

Where I_p is the desired current intensity of the pulse, R_{bank} the equivalent series resistance of the capacitor bank and R_L the TF coils resistance value which is 10 mΩ according to Table 2.3. Contrarily to the minimum voltage, there are many possible values for the maximum voltage of the CB, but only one that minimizes the number of CCs needed. This optimal maximum voltage also depends on the values of the 3 parameters that were presented before: desired current intensity, pulse duration and selected cells, therefore, the solution is only optimized for the particular situation for which the CB was sized. The ideal maximum voltage was calculated with and without considering the internal resistance of the supercapacitor cells.

Maximum Voltage Without Considering the Internal Resistance of the Cells

For a better understanding, the process will be first performed and explained without the parasitic resistance of the cells. The maximum voltage determines the number of CCs in series. The higher this value is the higher the variation of voltage during the discharge, therefore, the greater the amount of energy stored that is used (useful energy). This concept is explained by

$$E_u = \frac{1}{2}C_{bank}(V_{max}^2 - V_{min}^2) \tag{4.4}$$

Where E_u is the useful energy, C_{bank} the capacitance of the bank, and V_{max} the maximum voltage. However, it is necessary to have enough cells in parallel to supply the desired pulse current, thus the minimum number of CCs in parallel that satisfy the power demand is given by

$$Np_{minP} = ceil\left(\frac{I_p}{0.8AMC_c}\right) \tag{4.5}$$

Where AMC_c is the absolute maximum current of each selected CC, 0.8 corresponds to a safety margin of 20 % and the $ceil$ (ceiling) is the smallest integer greater than or equal to the element. The total number of cells needed where computed for a range of values with increments of 1 V on the maximum voltage. The first step is to compute the number of CCs in series, this is

$$Ns = ceil\left(\frac{V_{max}}{V_r}\right) \tag{4.6}$$

Where V_r is the rated voltage of each CC. Afterwards, it is computed the energy dissipated in the resistance of the TF coils during the operation period. This energy is the useful energy that the capacitor bank needs to supply, and it is calculated using (4.2). After obtaining the energy dissipated during the pulse, the capacitance of the CB is computed by rearranging (4.4) and replacing the useful energy (E_u) by the energy of the pulse (E_p), resulting in

$$C_{bank} = \frac{2E_p}{V_{max}^2 - V_{min}^2} \tag{4.7}$$

The number of CCs must be enough to obtain the required capacitance, computed from (4.7), therefore the minimum number of cells in parallel needed to satisfy the energy demand is obtained considering this capacitance and the number of cells in series, which is given by

$$Np_{minE} = ceil\left(\frac{C_{bank}Ns}{C_c}\right) \tag{4.8}$$

Where C_c is the capacitance of each CC. Finally, the number of CCs in parallel is determined considering the minimum requirement to meet the current or power demand, from (4.5), and the minimum requirement to meet the energy demand, from (4.8), as follows:

$$Np = max\left(Np_{minP}, Np_{minE}\right) \tag{4.9}$$

Where max is the greater value between the two elements. This means that the number of cells can be either limited by power or energy demand. Figure 4.1 shows the total number of cells for different maximum voltages (with increments of 1 V), considering a current pulse of 8500 A with 3 s, and SCA3200 cells (3200 F). The parameters of the CCs are presented in Table 2.6.

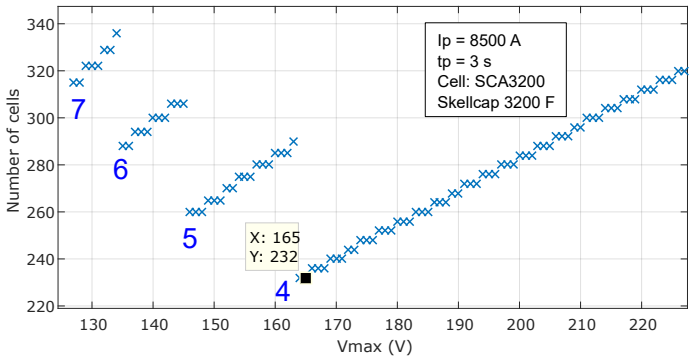

Figure 4.1: Number of CCs with respect to maximum voltage (CCs without internal resistance).

According to Figure 4.1, the optimal maximum voltage in this situation is 164 V and 165 V (both lead to the same number of CCs in series). The blue numbers near each cluster correspond to the number of parallel cells needed. In conclusion, if the internal resistance of the CCs is not taken into account, the optimal solution must have the minimum number of cells in parallel that are sufficient to supply the required current of the pulse, this is expected.

Maximum Voltage Considering the Internal Resistance of the Cells

If the internal resistance is taken into consideration this reasoning becomes invalid because as the number of cells in series increases the equivalent series resistance (ESR) of the CB also increases. This internal resistance is given by

$$R_{bank} = \frac{ESR_c Ns}{Np} \tag{4.10}$$

Where R_{bank} is the ESR of the capacitor bank and ESR_c the ESR of each CC. The useful energy that the CB must provide is now the sum of the dissipated energy in the coils, given by (4.2), and the dissipated energy in the equivalent series resistance of the bank, this is

$$E_u = E_p + R_{bank} I_p^2 t_p \tag{4.11}$$

The capacitor bank is sized based on 5 equations: (4.3), (4.4), (4.8), (4.10) and (4.11) which establish the following system of equations:

$$\begin{cases} V_{min} = I_p(R_L + R_{bank}) \\ E_u = \frac{1}{2} C_{bank}(V_{max}^2 - V_{min}^2) \\ C_{bank} = \frac{C_c Np}{Ns} \\ R_{bank} = \frac{ESR_c Ns}{Np} \\ E_u = E_p + R_{bank} I_p^2 t_p \end{cases} \tag{4.12}$$

This system can be simplified into one single nonlinear equation:

$$Np = 2 \frac{E_p + \frac{ESR_c Ns}{Np} I_p^2 t_p}{V_{max}^2 - (I_p(R_L + \frac{ESR_c Ns}{Np}))^2} \frac{Ns}{C_c} \tag{4.13}$$

This equation must be solved using an iterative method, in this case it was solved in MATLAB with respect to Np (number of cells in parallel). It is important to note that the value obtained from (4.13) needs to be rounded up to an integer. The total number of CCs were computed for different maximum voltages using (4.5) and (4.13). The results are presented in Figure 4.2 (a) for a current pulse of 8500 A with 3 s, and SCA0300 cells (300 F).

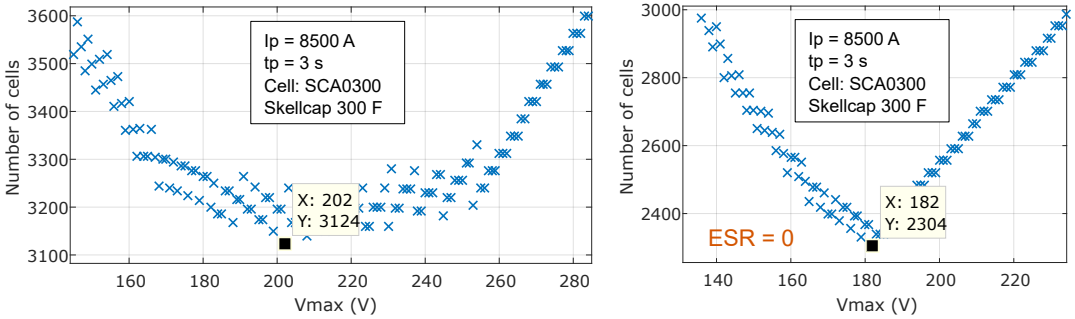

Figure 4.2: Number of CCs with respect to maximum voltage: (a) considering the ESR of the capacitors; (b) without the ESR.

Figure 4.2 also shows the impact of the internal resistance of the CCs, since Figure 4.2 (b) represents the same situation without considering the internal resistance. The optimal maximum voltage for these conditions is 202 V according to Figure 4.2 (a), which corresponds to 71 cells in series and 44 cells in parallel. The same computations were conducted for different current pulses and different types of CCs. Figure 4.3 represents the total number of cells needed for a pulse of 15000 A with 3 s (a) and a pulse of 6000 A with 10 s (b), both using SCA0300 cells (300 F). Also, Figure 4.4 illustrates the same situation but now considering bigger cells, SCA3200 (3200 F).

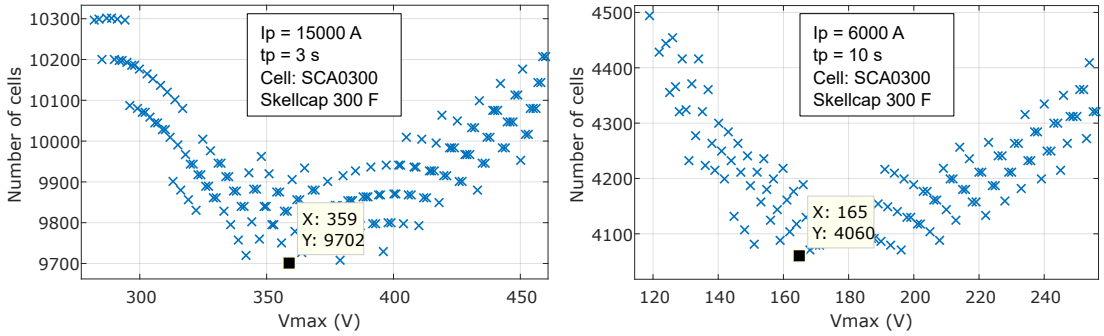

Figure 4.3: Number of CCs with respect to maximum voltage, using SCA0300 cells, for a pulse of: (a) 15000 A with 3 s; (b) 6000 A with 10 s.

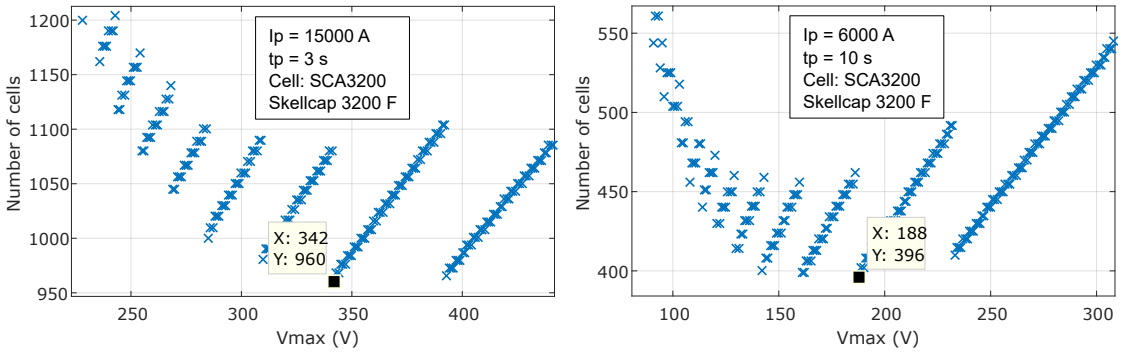

Figure 4.4: Number of CCs with respect to maximum voltage, using SCA3200 cells, for a pulse of: (a) 15000 A with 3 s; (b) 6000 A with 10 s.

Parameters of the Supercapacitor Bank

After obtaining the maximum voltage which minimizes the number of CCs for a particular situation, it is possible to determine the parameters of the resulting capacitor bank. This results are computed based on the equations that were already presented in addition to the following equations. The capacitance of the bank is given by

$$C_{bank} = \frac{C_c N p}{N s} \tag{4.14}$$

And the total energy that the capacitor bank (E_{bank}) is able to store is given by

$$E_{bank} = \frac{1}{2} C_c V_r^2 N_c \tag{4.15}$$

Where N_c is the total number of cells. It is also important to compute the energy left in the CB at the end of the pulse, which is given by

$$E_{left} = E_{bank} - E_u \tag{4.16}$$

Where E_u is the useful energy that the bank must be able to supply, that is equal to the dissipated energy in the coils and the internal resistance of the CCs, described by (4.11). The energy left in percentage is obtain by dividing the energy left (E_{left}) by the total energy stored (E_{bank}). Another relevant parameter is the absolute maximum current of the CB, given by

$$AMC = AMC_c Np \tag{4.17}$$

Where AMC_c is the maximum current of each CC. The parameters of the capacitor bank are presented in Table 4.2 for the different situations represented in Figure 4.2, 4.3 and 4.4.

Table 4.2: Parameters of the optimized capacitor bank for different situations. Considering 3 different pulses and 2 types of cells.

ID	Ip (A)	tp (s)	Cell	Vmax (V)	Ns	Np	Nc	Cbank (F)	Rbank (mΩ)
1	8500	3	SCA0300	202	71	44	3124	185.9	2.58
2	15000	3	SCA0300	359	126	77	9702	183.3	2.62
3	6000	10	SCA0300	165	58	70	4060	362.1	1.33
4	15000	3	SCA3200	342	120	9	960	213.3	2.70
5	6000	10	SCA3200	188	66	6	396	290.9	1.98

ID	Ep (MJ)	Eu (MJ)	Ebank (MJ)	Eleft (MJ)	left(%)	AMC (kA)	Ed (MJ)	x(%)
1	2.17	2.73	3.81	1.08	28.4	13.2	0.56	57.0
2	6.75	8.52	11.82	3.30	27.9	23.1	1.77	57.1
3	3.60	4.08	4.95	0.87	17.6	21.0	0.48	72.7
4	6.75	8.57	12.48	3.90	31.3	24.8	1.82	54.1
5	3.60	4.31	5.15	0.83	16.2	18.6	0.71	69.9

The ID is the identification for each particular circumstances, in this case, the analysis was carried out for 5 different situations. The percentage of energy left is a common way to measure the performance of a CB, the smaller this value is the better, however, it has to be taken into account that part of the energy that was discharged from the bank was dissipated in its own resistance (ESR), the amount of energy dissipated in the CCs is represented in Table 4.2 by Ed (MJ). Therefore, a better way to measure the performance is comparing the energy required for the pulse (Ep), with the energy stored in the capacitor bank (Ebank), this is represented by the

variable x (%) in Table 4.2, which is the ratio between these two values. The sum of the energy dissipated in the capacitors and the energy left is the amount of energy that was not used to supply the TF coils during the pulse. The situations where the capacitor bank performs better correspond to the IDs 3 and 5, this is expected since it is the pulse with more duration. The situation where the CB performs worst is identified by the ID 4, and corresponds to the pulse with the highest current intensity and bigger cells. In conclusion, as the duration of the pulse increases the CB needed also increases (since the pulse requires more energy), however, the performance increases too because the losses in the equivalent series resistance (ESR) of the CB decreases.

Operation for Different Current Pulses

Now that the optimization process of the capacitor bank has been studied, it is important to analyse the performance of the bank for current pulses that are different from the one that was used to size the CB. For example, the CB with ID = 1 in Table 4.2 was optimized for a current pulse of 8500 A with 3 s, however, it is essential to determine for different current intensities the duration of the pulse that the CB is able to withstand. This is represented in Figure 4.5.

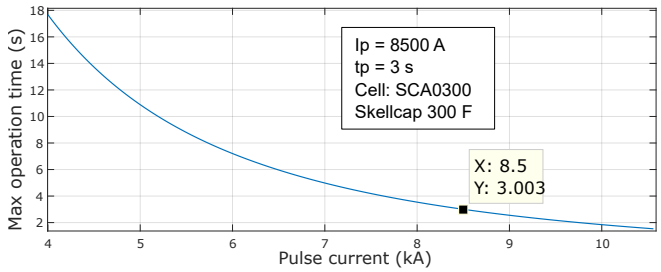

Figure 4.5: Maximum pulse duration with respect to pulse current intensity for the CB with ID = 1.

The minimum current represented is 4000 A which corresponds to the minimum value of the toroidal magnetic field with concern to the project. The maximum current represented is the maximum current that the capacitor bank is able to supply, which is equal to 80 % of the absolute maximum current of the bank. The same computations were conducted for other CBs, Figure 4.6 shows the operation under different conditions of the capacitor banks with ID = 2 and ID = 3.

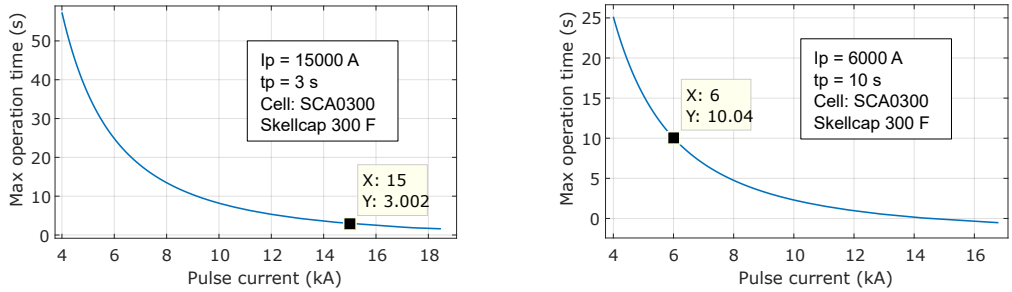

Figure 4.6: Maximum pulse duration with respect to pulse current intensity for: (a) CB with ID = 2; (b) CB with ID = 3.

New Power Supply of the Supercapacitor Bank

The supercapacitor bank is charged during the interval between pulses by a new DC source, which is responsible to set the voltage of the CB to the reference level. The maximum output voltage of the power supply depends on the CB that was sized before, more specifically depends on the maximum voltage of the CB. The output power requirement for the source P_{out} is given by

$$P_{out} = \eta \frac{E_{bank}}{t_{rest}} \tag{4.18}$$

Where η is the efficiency of the charging process, E_{bank} the total energy stored by the capacitor bank and t_{rest} the interval between pulses. Considering an efficiency of 90 $\%$ and a rest period of 15 min, for the CB with the ID = 1 (from Table 4.2) the power supply must have an output power of at least 4.7 kW. Regarding the maximum voltage of the DC source for the same CB the value is approximately 202 V. Since the rest period is much longer than the pulse duration, the output power requirement for the power supply is much smaller than the output power of the CB. As a result, this solution highly decreases the contracted power tariff of the system.

4.3.2 Optimal Sizing of the Electrolytic Capacitor Bank (ECB)

In order to design a circuit able to recover the energy left in the TF coils it is crucial to size the storage system properly. The capacity of this ESS only needs to be enough to store the remaining magnetic energy, but unlike the supercapacitor bank, does not need to provide all the energy for the current pulse. The losses that result from the energy transfer between the coils and the capacitor bank must be minimized. This losses are related with the internal resistance of the components. As a result, the capacitance of the CB must lead to voltages that minimize the resistive losses. This transfer process happens within time intervals in the order of milliseconds which can be computed using (2.17).

The first attempt was to use supercapacitors just like before, and associate the capacitor cells (CC) mainly in series in order to reduce the capacitance value and increase the voltage that the CB was able to withstand. However, this solution is unfeasible because the rated voltage of this type of cells is very low, resulting in too many cells in series. Consequently, the equivalent series resistance becomes to big which leads to very high voltage drops across the internal resistances of the supercapacitors. As a result, the CCs charge insufficiently (less than 10 %). This is expected since supercapacitors are not capable of fully charging and discharging within periods in the order of milliseconds. However, electrolytic capacitors are capable, this is why they are the selected technology to store the remaining energy on the TF coils.

Maximum Voltage of the Electrolytic Capacitor Bank

The maximum voltage determines how many cells in series are needed. The higher this number is the smaller the capacitance value of the CB, which is described by (4.14). Generally, a higher maximum voltage corresponds to fewer losses during the recovery process to some extent. Nevertheless, the voltage of the ECB must not be excessive, otherwise it might potentially harm the other components of the system like the semiconductor devices. It is also required to have enough CCs in parallel to withstand the current intensity. Table 4.3 presents approximately the efficiency of the energy transfer from the coils to the ECB for different maximum voltages. These values can be obtained either by simulation, for example using the circuit represented in Figure 4.12, or by analytical means which will be covered further.

Table 4.3: Efficiency of the recovery process with respect to maximum voltage.

Maximum voltage (V)	400	800	1200	1600
Efficiency (%)	75	84	88	89

From Table 4.3 it is possible to verify that the efficiency for 1200 V and 1600 V is almost the same, thus, it is preferable to have a maximum voltage lower than 1200 V to avoid damage to the system components. The efficiency using 800 V is slightly lower, but taking into consideration the risks of higher voltages, 800 V is probably the most suitable maximum voltage for the ECB.

Parameters of the Electrolytic Capacitor Bank

The parameters of the ECB are computed in a similar way to the ones of the supercapacitor bank from subsection 4.3.1. Starting with the number of CCs in series the value is obtained using (4.6). The ECB needs enough storage capacity to be able to store the magnetic energy left in the TF coils at the end of the pulse. However, part of this magnetic energy is dissipated during the recovery process, therefore, the ECB is sized to store a little less energy than the coils. The required storage capacity is calculated by multiplying the efficiency of the recovery process by the total energy stored in the coils, which is expressed by

$$E_{ECB} = \eta E_L \tag{4.19}$$

Where E_{ECB} is the maximum energy that the ECB must be able to store, and E_L is the maximum magnetic energy stored in the coils which is obtained using (2.1). There are two ways to compute the efficiency: by using the results of the simulations, or by using the concepts of the RLC circuit that were presented in section 2.6. Both processes are iterative, consequently, the first iteration is carried out considering the efficiency equal to 1. Table 4.3 was made using the first method. The second way is to compute the efficiency using the losses during the recovery process, which is given by

$$\eta = \frac{E_L - E_{loss}}{E_L} \tag{4.20}$$

Where E_{loss} is the energy dissipated in the internal resistance of the components, given by

$$E_{loss} = \int_0^{t_d} (R_L + R_{ECB}) i^2(t)\, dt \tag{4.21}$$

Where R_L is the resistance of the TF coils, R_{ECB} is the equivalent series resistance of the ECB, t_d is the discharge time computed from (2.17), and $i(t)$ the time-varying current flowing through the coils during the recovery process which is expressed by (2.15). After replacing the expression of the current on the equation (4.21) it is obtained

$$E_{loss} = \int_0^{t_d} (R_L + R_{ECB}) Ip^2 \cos^2(\omega_0 t)\, dt \tag{4.22}$$

After computing the maximum energy that the ECB must be able to store (E_{ECB}), the minimum capacitance of the capacitor bank required to meet this energy demand (C_{ECBmin}) is given by

$$C_{ECBmin} = \frac{2E_{ECB}}{V_{max}^2} \tag{4.23}$$

Where V_{max} is the maximum voltage of the capacitor bank. Finally the number of CCs in parallel required is obtained using

$$N_p = ceil\left(\frac{C_{ECBmin} Ns}{C_c}\right) \tag{4.24}$$

Where C_c is the capacitance of each CC, the parameters of the cells are presented in Table 2.7. The capacitance of the ECB is computed using (4.14). The ESR of the bank is computed using (4.10). Considering a maximum current intensity of 8500 A, and a maximum voltage for the ECB of 800 V, the value obtained for the capacitance is 187.5 mF.

4.3.3 Theoretical Circuit Schematic and Operation States

The connection between the capacitor bank and the TF coils is carried out using a power converter capable of charging the TF coils and recovering the remaining energy. In addition, the converter must be able to use the recovered energy in the next current pulse. For this application, the power must flow in both directions, either from source to load or load to source. The current flowing though the coils has always the same direction. During the pulse the CB feeds the TF coils (load) consequently, the voltage has the same direction of the current. At the end of the pulse the coils, which have a large inductance value, oppose the change in current, therefore the polarity of the voltage is inverted and the coils must discharge to the CB. This implies that the circuit must operate in the first and fourth quadrant, characterised by positive current and both positive and negative voltage.

As a result, the first circuit selected capable of operating like this is the two-quadrant voltage reversible chopper. This circuit is represented in Figure 4.7 (a), furthermore it is represented the DC source responsible for charging the CB during the interval between pulses. Figure 4.7 (b) shows an upgrade to the first converter. The second circuit was inspired in the two-quadrant voltage reversible chopper, modified so that the recovered energy is only delivered to the storage capacitance C1. Both circuits operate in 4 different states which are represented respectively in Table 4.5 and Table 4.4.

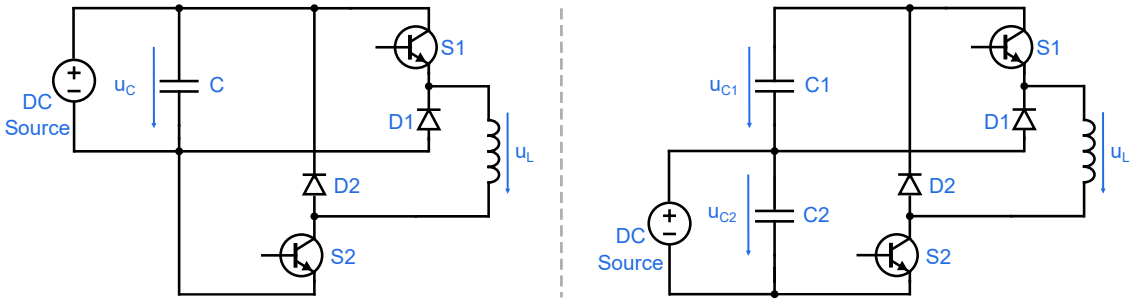

Figure 4.7: Circuit based on the voltage reversible two-quadrant chopper (type D chopper).

Table 4.4: Voltage across the inductor for all states of the first circuit.

State	S1	S2	u_L without voltage drop	u_L with voltage drop
1	OFF	OFF	$u_L = -u_C$	$u_L = -u_C - u_{D1} - u_{D2}$
2	ON	OFF	$u_L = 0$	$u_L = -u_{S1} - u_{D2}$
3	OFF	ON	$u_L = 0$	$u_L = -u_{S2} - u_{D1}$
4	ON	ON	$u_L = u_C$	$u_L = u_C - u_{S1} - u_{S2}$

Table 4.5: Voltage across the inductor for all states of the second circuit.

State	S1	S2	u_L without voltage drop	u_L with voltage drop
1	OFF	OFF	$u_L = -u_{C1}$	$u_L = -u_{C1} - u_{D1} - u_{D2}$
2	ON	OFF	$u_L = 0$	$u_L = -u_{S1} - u_{D2}$
3	OFF	ON	$u_L = u_{C2}$	$u_L = u_{C2} - u_{S2} - u_{D1}$
4	ON	ON	$u_L = u_{C1} + u_{C2}$	$u_L = u_{C1} + u_{C2} - u_{S1} - u_{S2}$

Regarding Figure 4.7, the inductor L represents the TF coils, and the voltage across the inductor is expressed with and without taking into consideration the voltage drop across the semiconductors (Diodes and Switches). The capacitor C1 and C2 will be explained in the next subsections where the implementation of these converters will be covered. Since the first circuit is a conventional and popular converter its states will not be presented in detail. Regarding the second circuit, the first state occurs when both switches (S1 and S2) are open, as a result, the voltage across the inductor L is equal to the negative of the voltage on the first capacitor (C1). During this state, the

inductor L discharges to the capacitor C1 through the diodes (D1 and D2). The second state occurs when the switch S1 is closed, as a result, the inductor is short circuited. During this state, the magnetic energy is dissipated in the internal resistance of the inductor and the semiconductors (S1 and D2). The third state occurs when the switch S2 is closed, as a result, the voltage across the inductor is equal to the voltage on the second capacitor (C2). During this state, the capacitor C2 discharges to the inductor through the semiconductors (S2 and D1). Lastly, the fourth state occurs when both switches (S1 and S2) are closed, as a result, the voltage across the inductor is equal to the sum of the voltage on both capacitors. During this state, the capacitors are in series and discharge to the inductor through the switches (S1 and S2).

4.3.4 Supercapacitor Power Supply Without Electrolytic Capacitor Bank

The first circuit that was implemented was the regular voltage reversible chopper shown in Figure 4.7 (a). The capacitor C represents the supercapacitor bank which is sized based on the principles presented in subsection 4.3.1. Figure 4.8 represents the implementation of this circuit in Simulink, which can be divided into two parts. The left part (a) is the main circuit or the power circuit which includes the CB, the coils and the converter, and the right part (b) is the control circuit. The CB is implemented using an ideal capacitor (C) with the required capacitance and a resistor which represents the equivalent series resistance of the bank (Rc). The DC source is represented by the voltage source Vs and the internal resistor Rs. This power supply can be neglected during the pulse because its output power is much lower than that of the CB.

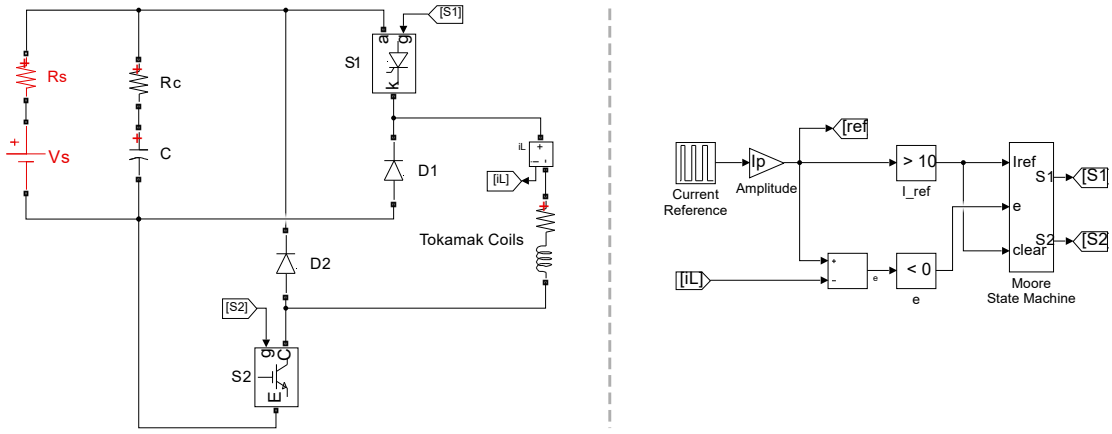

Figure 4.8: [Circuit 1.1] Supercapacitor power supply without electrolytic capacitor bank: (a) power circuit; (b) control circuit.

The control circuit (low power) shown in Figure 4.8 (b) is responsible for providing the control signals to the semiconductor switches (S1 and S2), in this case, IGBTs. This circuit has two inputs: the current reference which corresponds to the desired amplitude and duration of the pulse, and the intensity of the current that flows through the TF coils measured by a current transformer. The error of the current is the difference between the reference and the value of the current measured.

The states of the circuit and the transition between them are managed by a sequential circuit, in this case, a Moore State Machine. This machine receives two binary inputs, one that indicates if the current reference is positive and the other indicates if the current error is negative which means that the current measured is greater than the desired pulse intensity. These binary inputs come from two comparison blocks. The state machine also needs a clock signal to control the transition between states. The operation of the circuit is represented in Figure 4.9 at the initial stage of the pulse defined by the current rising (a), and at the final stage of the pulse defined by the current falling (b), for a clock frequency of 10 kHz. The signal Iref is the current reference, and the signal IL is the current measured in the TF coils for a pulse of 8500 A with 3 s.

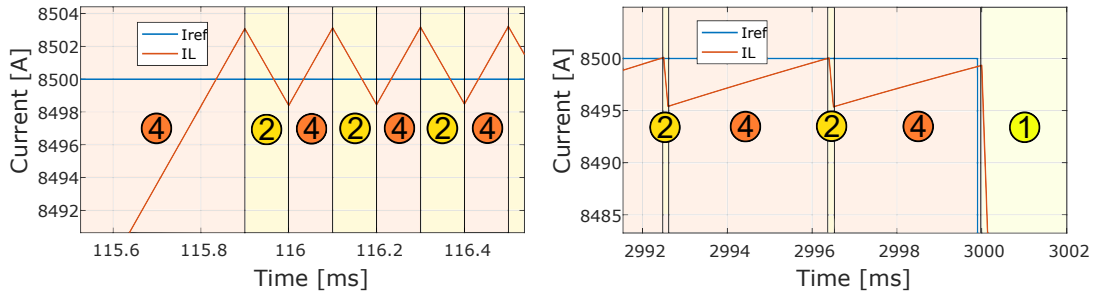

Figure 4.9: Operation of the first circuit and its states at: (a) the beginning of the pulse; (b) the end of the pulse. Current ripple and reference.

The numbers inside the circles indicate in which state the circuit is operating, these states were presented in Table 4.4. During the pulse the current reference is positive, hence the circuit alternates between two states (2 and 4) according to the error of the current. State 2 is used to decrease the intensity of the current flowing through the coils when the current measured is superior to the reference (negative current error). Oppositely, state 4 is used to increase the intensity of the current when the current measured is less than the desired current (positive current error). At the end of the pulse, the magnetic energy stored in the coils is injected into the capacitor bank, therefore, the circuit operates in the state 1. Figure 4.9 also shows that the shape of the current is slightly different at the beginning and at the end of the pulse, due to the variation on the voltage of the CB during the discharge. The ripple of the current also depends on the clock frequency value. Figure 4.9 was obtained for a clock frequency of 10 kHZ which corresponds to a clock period of 100 μs. The higher the frequency is the greater the number of transitions between states, therefore, the current ripple is smaller because the state is updated more times. Table 4.6 shows the peak current deviation from the reference for different clock frequencies considering a pulse of 8500 A with 3 s. It also shows the number of times the semiconductor S2 switches (turns on or turns off), this is a relevant parameter because semiconductors have commutation losses.

Table 4.6: Maximum current deviation and number of commutations with respect to clock period.

Clock period (us)	50	100	200	400
Peak current deviation (A)	2.36	4.71	9.43	18.72

Simulation of the Circuit and Waveforms

Now that the control circuit and the transitions between states have been covered, the main simulation results for a pulse reference of 8500 A with 3 s will be presented. The capacitor bank (CB) was sized based on the concepts presented in subsection 4.3.1, in this case it corresponds to the situation with ID = 1 in Table 4.2. Starting with the current flowing through the TF coils, Figure 4.10 (a) represents the reference (Iref) and the actual current measured (IL). It also shows how much time it takes for the coils to get to the desired current intensity. It takes approximately 116 ms for the current to rise to 8500 A and 98 ms for the current to drop to 0 A. Figure 4.10 (b) shows the voltage across the coils during the pulse. The initial voltage applied to the coils corresponds to the parameter Vmax of the CB in Table 4.2 which is 202 V for this situation. As mentioned before, the discharge curve of the capacitors is not flat which means that the voltage decreases as the energy is used up. During the pulse the voltage is constantly fluctuating, which can be observed in Figure 4.10 (b), because the circuit is alternating between two states of operation, state 2 and 4. At the end of the pulse (3000 ms) the polarity of the voltage is inverted (-137.1 V) which means that the coils inject the energy back into the circuit, more precisely into the CB.

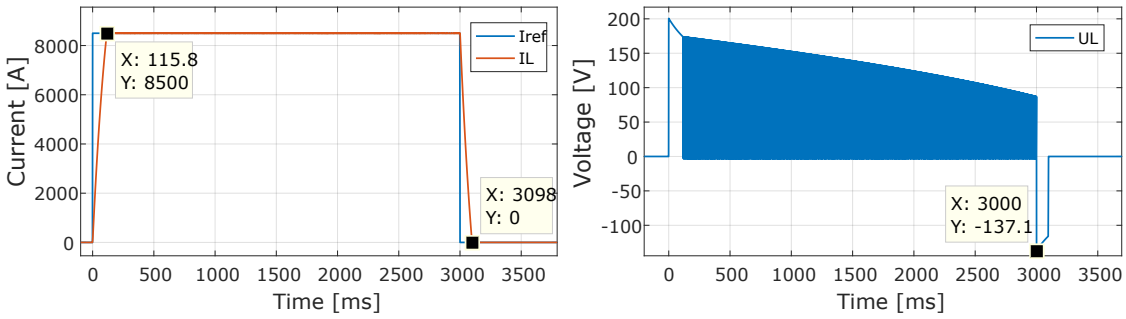

Figure 4.10: Simulation results for a pulse of 8500 A with 3 s: (a) current flowing through the TF coils; (b) voltage across the coils. No initial transient, better waveform.

Regarding the CB, this element is implemented using an ideal capacitor and a resistor. It is relevant to analyse the progression of the voltage at the terminals of the CB, this is represented in Figure 4.11 (a). The voltage has a strong ripple during the pulse due to the voltage drop on the internal resistance of the CB. When the capacitor is feeding the coils (state 4) the voltage drop is nearly 22 V, this can be verified by making the difference between the values of the voltages shown in Figure 4.11 (a), or by multiplying the value of the desired current (8500 A) by the equivalent series resistance of the CB. At the end of the pulse the voltage increases because the coils are now supplying the CB (state 1), thus, part of the magnetic energy left in this inductor is reused to

charge the bank. The energy injected into the CB can be computed using (2.8) with the values of the voltage measured across the capacitor bank without including the voltage drop on the internal resistance (voltage of the ideal capacitor), which is illustrated in Figure 4.11 (b). Take note that in practice, it is impossible to obtain this graphic however, the voltage values needed to compute the energy recovered can be also acquired from Figure 4.11 (a).

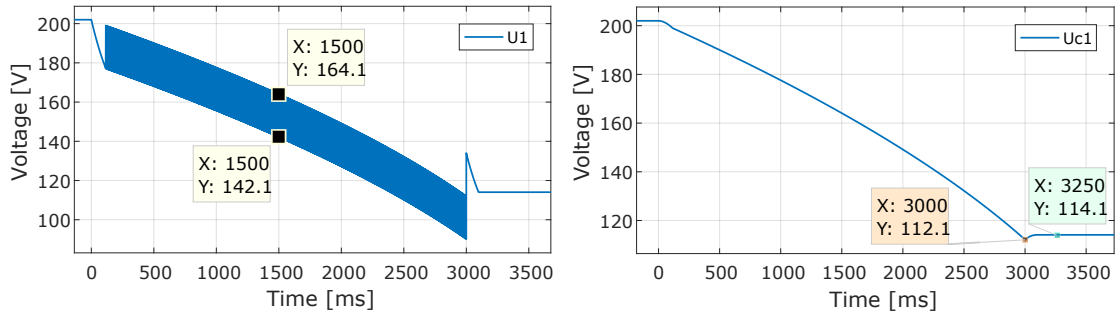

Figure 4.11: Evolution of the voltage across the capacitor bank: (a) with voltage drop across the internal resistance; (b) without voltage drop.

Regarding the equation (2.8) it is necessary to determine the final voltage (V_f) and initial voltage (V_i), this values are obtained from Figure 4.11. The voltage of the CB at the end of the pulse (instant 3000 ms) is 112.1 V and corresponds to the initial voltage of the charging process, when the coils fully discharge the voltage increases to 114.1 V where it stabilizes and corresponds to the final voltage. In this case, the energy that is returned to the CB is approximately 42 kJ and corresponds to about 65 % of the magnetic energy left in the TF coils at the end of the pulse (Table 4.1). The energy that is not used to charge the CB is dissipated in the internal resistance of the coils and the ESR of the capacitor bank.

4.3.5 Supercapacitor Power Supply With Electrolytic Capacitor Bank

The second circuit that was implemented is represented in Figure 4.7 (b). The capacitor C2 represents the supercapacitor bank, and the capacitor C1 represents an electrolytic capacitor bank (ECB). The purpose of adding an ECB is to obtain better rise and fall times for the output pulse current, and to recover more energy. The sizing of the ECB is covered in subsection 4.3.2. Figure 4.12 represents the implementation of this circuit in Simulink, which like the other can be divided into the power part (a) and the control part (b). Rc1 and Rc2 are the equivalent series resistance of the CBs. The DC source used to charge the supercapacitor bank between the pulses is represented by the voltage source Vs and the internal resistor Rs.

The state machine of the control circuit is similar to the one used in the first circuit, however, in addition to the two binary inputs from before, positive current reference and negative error, there is now a third which indicates if the ECB is charged. The operation of the circuit and the transitions between states is also identical to the first circuit and it is represented in Figure 4.13, at the beginning of the pulse (a) and at the end (b) for a clock frequency of 10 kHz.

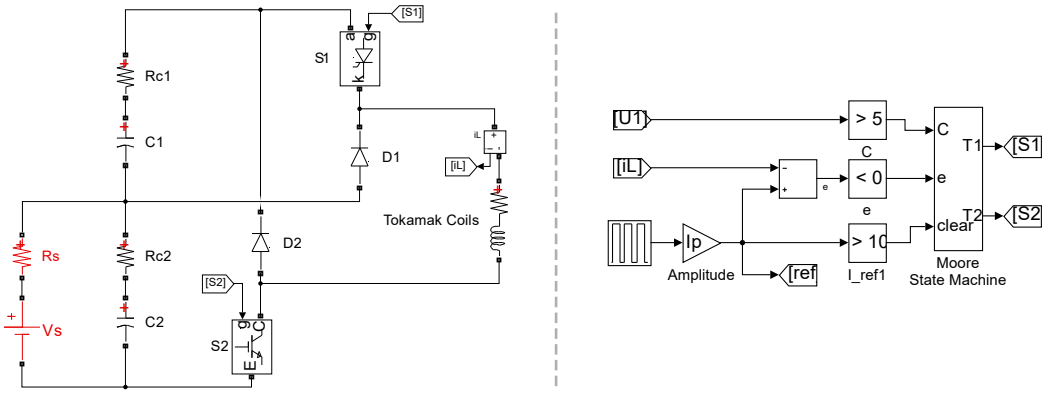

Figure 4.12: [Circuit 1.2] Supercapacitor power supply with an electrolytic capacitor bank: (a) power part; (b) control part.

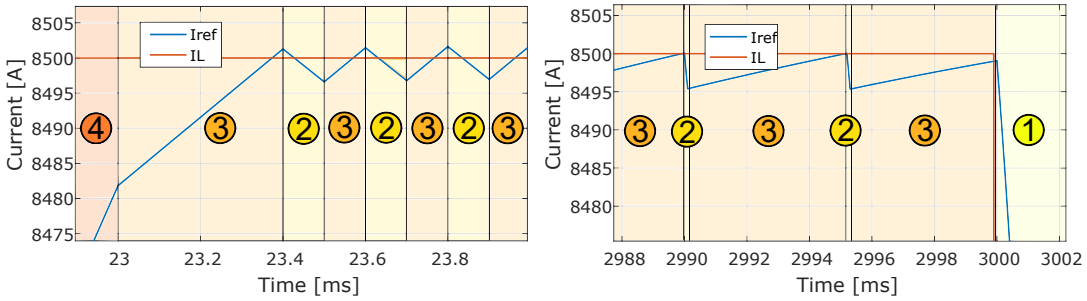

Figure 4.13: Operation of the second circuit and its states at: (a) the beginning of the pulse; (b) the end of the pulse. Current ripple and reference.

At the beginning of the pulse, if the ECB is charged the circuit will operate in the state 4 which means that both CBs will discharge in series to the coils. When the ECB fully discharges the circuit starts operating in the state 3, this transition is represented in Figure 4.13 (a). During the steady part of the pulse, the circuit alternates between two states according to the error of the current: state 2 and 4 if the ECB is still charged, and state 2 and 3 if the ECB is discharged. In this case, the ECB discharges during the rise of the current thus, in the steady part of the pulse the circuit alternates between state 2 and 3. State 2 is used to decrease the intensity of the current flowing through the coils (negative current error) and state 3 and 4 is used to increase the intensity of the current (positive current error). Finally, at the end of the pulse, the magnetic energy stored in the coils is used to charge the ECB, therefore, the circuit operates in the state 1.

Simulation of the Circuit and Waveforms

Now it will be presented the main simulation results of the second circuit for the same pulse and supercapacitor bank used in the first circuit, which corresponds to the situation with ID 1 in Table 4.2. Starting with the current flowing through the TF coils, Figure 4.14 represents the reference (Iref) and the actual current measured (IL). It takes approximately 23 ms for the current to rise to 8500 A and 28 ms for the current to drop to 0 A, this is considerably faster than the previous circuit

which can be verified by comparing with the Figure 4.10 (a). Figure 4.14 (b) shows the voltage across the coils during the pulse. The initial voltage applied to the coils corresponds to the sum of the voltages at the terminals of the supercapacitor bank (C2) and the ECB (C1). The ECB was sized to withstand 800 V (nominal voltage), therefore, the initial voltage across the coils is very high (980.9 V) which is why the rise time of the current was shortened so much in relation to the first circuit. The higher the voltage applied to the coils the less time it takes to energize them. At the end of the pulse (3000 ms) the polarity of the voltage is inverted reaching -782.2 V.

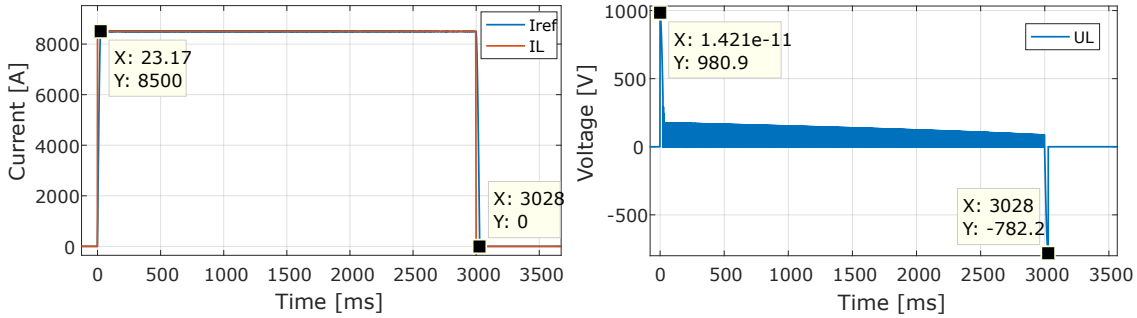

Figure 4.14: Simulation results for a pulse of 8500 A with 3 s: (a) current through the TF coils; (b)voltage across the coils. Reduced current rise and fall times.

The evolution of the voltage at the terminals of the CBs is represented in Figure 4.15, for the ECB (a) and the supercapacitor bank (b). The ECB discharges at the beginning of the pulse and charges at the end reaching 780.8 V. The capacitance value of the ECB is 187.5 mF, this value was obtained based in subsection 4.3.2, considering a maximum current of 8500 A. Knowing the voltage variation and the capacitance it is possible to compute the energy injected into the ECB during the charging process using (2.8). In this case, the energy that is returned to the CB is approximately 57 kJ and corresponds to about 84 % of the magnetic energy left in the TF coils at the end of the pulse. Comparing the energy recovered in both circuits the second circuit (with ECB) recovers almost 20 % more energy than the first. The voltage across the supercapacitor bank is represented in Figure 4.15 (b). The waveform is similar to the one illustrated in Figure 4.11 (a), except this time, the CB does not charge at the end of the pulse.

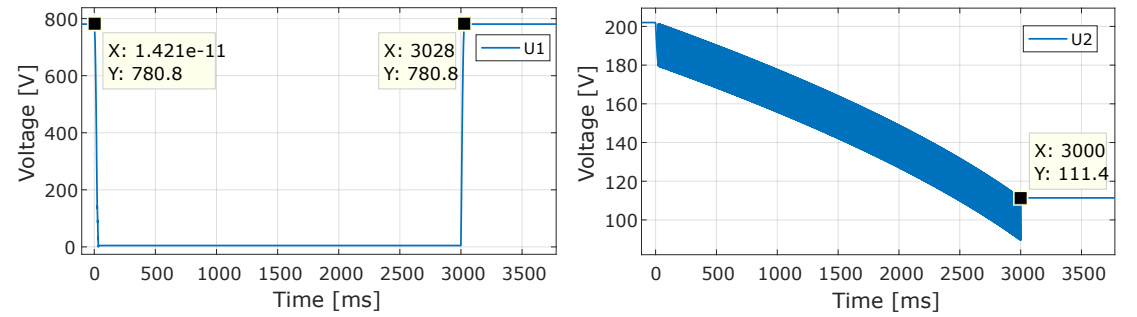

Figure 4.15: Evolution of the voltage across both capacitor banks: (a) electrolytic capacitor bank; (b) supercapacitor bank. Electrolytic capacitors charge and discharge in milliseconds.

4.4 Modified Rectifier Power Supply with Auxiliary Capacitor Banks (2nd Solution)

In this section, the possibility of modifying the configuration of the rectifier power supply and integrating a supercapacitor bank is assessed. The purpose of this solution is to increase the maximum current intensity of the pulse, using the existing power supply slightly modified. In order to achieve higher current pulses the output voltage of the power supply must be higher, as a result, the present rectifier configuration (parallel association of 4 three-phase rectifiers) must be modified. These three-phase rectifiers must be connected in series which results in an output voltage approximately 4 times higher than the standard configuration. However, the maximum current intensity will decrease 4 times, since the power limit has to be equivalent. Consequently, it is not enough to only change the power supply, this is why the integration of a supercapacitor bank is required. The CB must be sized in conjunction with the power supply to withstand the desired current intensity of the pulse. During the period between pulses the bank is charged using the same power supply. This solution is identical to the first one, but now the DC source that was only used to charge the CB between the pulses, is replaced with the existing rectifier which also operates during the pulse, reducing the power and energy demand on the supercapacitor bank.

4.4.1 Optimal Sizing of the Supercapacitor Bank

The sizing process of the CB is similar to the one described in section 4.3.1, however in this case, there is a power supply in parallel with the supercapacitor bank which also supplies the coils during the pulse. As a result, the CB does not need to be as big as before to provide the energy and power demand. Just like before, the capacitor bank is optimized for a specific combination of parameters: desired current intensity, duration of the pulse and the selected supercapacitor cell.

Minimum and Maximum Voltage of the Supercapacitor Bank

Together, the CB and the power supply must be able to sustain the desired current of the pulse during the defined time interval, this is only possible if the voltage of the supercapacitor bank is kept above a certain level (minimum voltage) during the pulse. The value of the minimum voltage is computed using the same process that was presented in subsection 4.3.1. Simply put, using (4.3). The maximum voltage of the capacitor bank is determined by the maximum voltage of the power supply. Regarding the output voltage of the rectifier, with the standard configuration, the average value is given by (2.2) and the peak value by (2.3). The 4 three-phase rectifiers are now connected in series instead of parallel, thus, the maximum voltage obtained at the output is approximately 378 V without considering the voltage drop on the thyristors. Contrarily to subsection 4.3.1, the maximum voltage is now a fixed value. In the first solution the voltage of the DC source was set in accordance to the optimized supercapacitor bank, that was sized first.

Parameters of the Supercapacitor Capacitor Bank

The parameters of the CB are computed using a similar procedure to the one used in subsection 4.3.1, the only differences are the fixed maximum voltage, and the rectifier power supply in parallel with the bank. The output current of the rectifier with standard configuration is limited to 8500 A, this restrain is imposed by the limitation on the power demand (from the public grid). This current intensity corresponds to nearly 723 kW of power supplied to the TF coils (shown in Table 4.1). If all the three-phase rectifiers are connected in series the current is limited to one fourth of the standard configuration or 2125 A, however, the maximum power fed by the rectifier is still the same as before, since the voltage is 4 times higher. Therefore, when sizing the CB it has to be taken into account the amount of energy that the power supply provides. The energy that the CB must deliver is given by

$$E_u = E_p + R_{bank} I_p^2 t_p - E_s \tag{4.25}$$

Where E_u is the useful energy that the CB must provide, E_p is the dissipated energy in the TF coils, R_{bank} is the ESR of the capacitor bank, I_p is the pulse current intensity, t_p the duration of the pulse and E_s the energy provided by the rectifier power supply. The higher this value, the less energy that the CB must supply, thus, the smaller the size of the bank. In order to obtain the smallest possible supercapacitor bank the computations must be conducted considering the maximum power that the rectifier source is able to supply (nearly 723 kW). The energy E_s is obtained by multiplying this power by the duration of the pulse.

The first parameter to be computed is the number of CCs in series (N_s), which is given by (4.6). The number of CCs in parallel (N_p) required to provide the energy demanded is obtained based on 5 equations: (4.3), (4.4), (4.8), (4.10) and (4.25). These equations can be simplified into one single nonlinear equation:

$$Np = 2\frac{E_p + \frac{ESR_c Ns}{Np} I_p^2 t_p - E_s}{V_{max}^2 - (I_p(R_L + \frac{ESR_c Ns}{Np}))^2} \frac{Ns}{C_c} \tag{4.26}$$

Where ESR_c is the ESR of each cell, C_c the capacitance of each cell and V_{max} the maximum voltage of the capacitor bank or rectifier. Just like before, this equation must be solved using an iterative method. The value of N_p obtained must be rounded up to the nearest integer. It is important to check if the number of CCs in parallel also meet the current or power demand, this can be verified by computing the minimum number of cells required using (4.5). After obtaining the total number of cells and their configuration, it is possible to determine the parameters of the resulting CB: the capacitance is given by (4.14), the ESR of the CB is given by (4.10) and the maximum energy stored is given by (4.15). The results obtained are presented in Table 4.7, in both situations considering a pulse of 15000 A with 3 s.

Table 4.7: Parameters of the capacitor bank sized for a pulse of 15000 A with different cells. Performance of the supercapacitor bank and losses.

ID	Ip (A)	tp (s)	Cell	Vmax (V)	Ns	Np	Nc	Cbank (F)	Rbank (mΩ)
1	15000	3	SCA0300	376	132	51	6732	115.9	2.59
2	15000	3	SCA3200	376	132	6	792	145.5	3.96

ID	Ep (MJ)	Eu (MJ)	Ebank (MJ)	Eleft (MJ)	left(%)	AMC (kA)	Ed (MJ)	x(%)
1	6.75	5.87	8.20	2.33	28.4	15.3	1.29	82.3
2	6.75	6.55	10.29	3.74	36.3	18.6	1.97	65.6

The parameters presented in Table 4.7 are the same ones presented in Table 4.2, the designation of the variables is also the same. In this case the capacitor bank is sized for a pulse of 15000 A, the reason behind this value is explained as follows. Given a fixed maximum voltage for the capacitor bank there are specific values for the pulse duration and current intensity that combined lead to an optimized CB, this means that the requisite for the power demand and the energy demand both lead to the same number of cells, thus the number of CCs is minimized. Considering a pulse duration of 3 s the current intensity that leads to a fairly optimized CB is approximately 15000 A. As the duration of the pulse increases, the energy demand becomes the limiting factor, since more cells are needed to supply the required energy for the pulse. If the duration decreases, the limiting factor becomes the power because although the energy needed is reduced, the current and the power that the capacitors must withstand is still the same.

4.4.2 Circuit Schematic and Operation States

The connection between the TF coils and the supercapacitor bank is carried out using the converter represented in Figure 4.16. This circuit schematic is the same one that was presented in subsection 4.3.3, with the exception that now the DC source is replaced with the 12-pulse rectifier connected in parallel with the supercapacitor bank (capacitor C2). The capacitor C1 represents the electrolytic capacitor bank (ECB) that is sized using the process that will be covered in subsection 4.3.2. The operation states of the circuit were already described in Table 4.5.

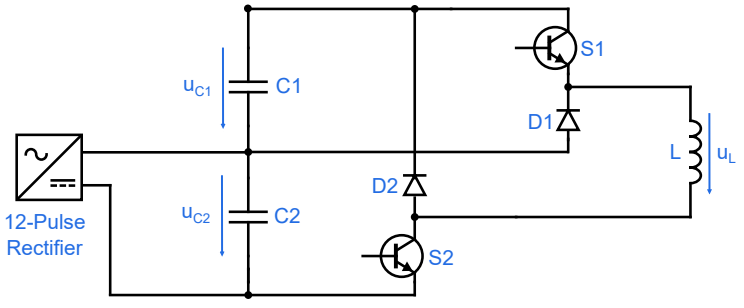

Figure 4.16: Theoretical circuit schematic for the second solution.

4.4.3 Implementation of the Circuit and Voltage Controller of the CB

This system was implemented in Simulink and the corresponding circuit can be divided into two parts: the modified power supply, and the connection between the elements of the circuit including the power converter. Starting with the 12-pulse rectifier, the schematic is represented in Figure 4.17. It is possible to verify that all the three-phase rectifiers are now connected in series, this is achieved by connecting the output of each rectifier system to the neutral of the secondary three-phase winding linked with the subsequent three-phase rectifier. The neutral points of the windings are located on the power transformers. The neutral of the first three-phase winding (n1), which is associated with the thyristors T1, T3 and T5, is connected to the ground. The output of the last three-phase rectifier, which includes thyristors T8, T10 and T12, is connected to an inductor named L_rect which is at the output of the rectifier power supply. The purpose of this inductor will be later explained. Now that the rectifiers are all connected in series (single branch) instead of parallel (four branches) there is no need to control the current of each three-phase rectifier individually. As a result, there is only one PI controller which regulates the output current.

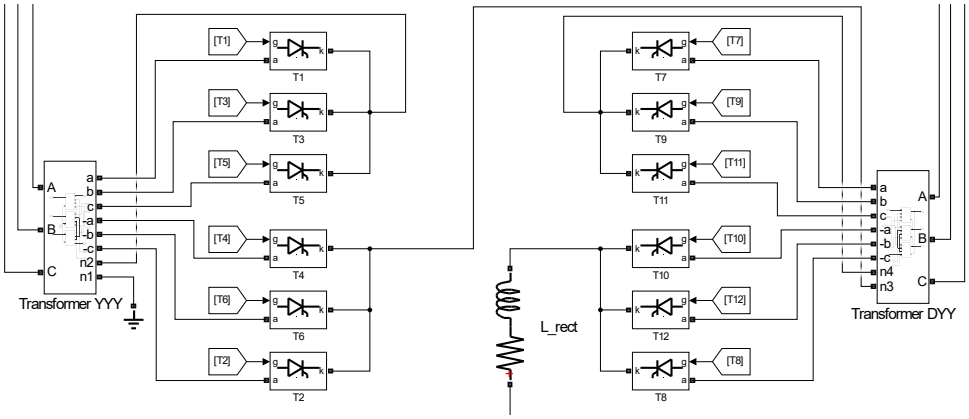

Figure 4.17: Circuit of the modified 12-pulse rectifier power supply, with the 4 three-phase rectifiers in series.

The second part of the circuit includes the connection between the rectifier, the CBs and the TF coils. The schematic of the circuit is represented in Figure 4.18. The block named 12_Pulse Rectifier is a subsystem containing the entire modified rectifier power supply which was already covered and illustrated in Figure 4.17.

This system can be divided into 3 parts: the power circuit, the control circuit and the capacitor voltage control circuit. The power circuit is the main circuit and includes all the major elements and semiconductor power devices. The control circuit (low power) is responsible for providing the control signals to the semiconductor switches (S1 and S2), this part includes the state machine. This control circuit is the same one that was used in Figure 4.12, consequently its operation was already covered in subsection 4.3.4. Finally, a controller for the capacitor voltage is added to the circuit because the supercapacitor bank is in parallel with the rectifier power supply. The purpose

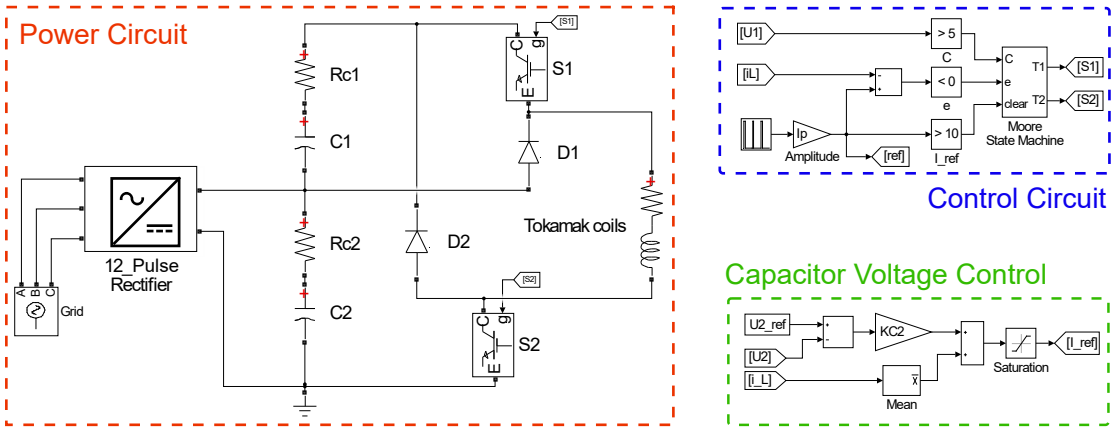

Figure 4.18: [Circuit 2] Implementation of the circuit for the second solution.

of this control system is to correctly charge the supercapacitor bank (C2 and Rc2), therefore, it is responsible for providing the current reference to the PI controller of the rectifier.

Controller for the Voltage of the Supercapacitor Bank

The capacitor voltage controller is a nonlinear system based on the Lyapunov stability principle. There are 3 equations that rule the controller. The first one describes the behavior of the circuit and it is obtained combining the constitutive equation of the capacitor with the current equation of the circuit (the current from the source is equal to the sum of the current entering the TF coils and the CB), this results in

$$C_2 \frac{dU2}{dt} = I_S - I_L \tag{4.27}$$

Where C_2 is the capacitance of the supercapacitor bank, $U2$ is the voltage across the bank, I_S the current supplied by the source, in this case the rectifier power supply, and I_L the current flowing though the TF coils. The second equation describes the error of the voltage of the CB which is the difference between the reference and the actual value, and is given by

$$e_{U2} = U2_{ref} - U2 \tag{4.28}$$

Where e_{U2} is the capacitor voltage error and $U2_{ref}$ is the voltage reference. For the controller to work properly, it is required a third equation to assure that the error converges to zero. This equation comes from the stability condition and it is given by

$$\frac{de_{U2}}{dt} = -Ke_{U2} \qquad (K > 0) \tag{4.29}$$

Where K is a positive gain. This equation guarantees that the value of the error increases (positive variation) when the error is negative, otherwise the error decreases (negative variation) when the error is positive. The value of K determines how fast the error converges to zero, the

inverse of this gain is equal to the time constant of the charging process. It takes approximately 5 time constants to fully charge the CB, in other words, to reach more than 99 % of the maximum voltage. The value of K is computed using the following equation

$$K = \frac{1}{\tau} < \frac{5}{t_{rest}} \tag{4.30}$$

Where τ is the time constant and t_{rest} is the rest period or the duration between pulses. The supercapacitor bank must fully charge during this period. Combining the equations (4.27), (4.28) and (4.29) it is obtained the fundamental equation of the voltage controller, given by

$$I_S = KC_2(U2_{ref} - U2) + C_2\frac{dU2_{ref}}{dt} + I_L \tag{4.31}$$

The derivative of a constant is equal to zero, thus the term of the equation with the derivative of the reference can be removed. The block of the capacitor voltage controller represented in Figure 4.18 results from this equation. The current I_S is the output of the capacitor voltage controller and it is the current reference (I_ref) of the PI controller.

4.4.4 Simulation of the Circuit and Waveforms

Now that the circuit has been explained, it is essential to analyse the results of the simulations. These results were obtained considering the CB that was sized in subsection 4.4.1, its parameters are presented in Table 4.7 and the CB is identified with the ID = 1. For the first simulation, it was considered a pulse with a current intensity of 15000 A and a duration of 3 s, these were the conditions used to size the CB. The main waveforms are represented in Figure 4.19, where U1 is the voltage of the ECB, U2 the voltage of the supercapacitor bank, Ip the current reference of the pulse, IL the current flowing through the TF coils, and Irect the current that the rectifier power supply is providing. Figure 4.19 was obtained considering an interval between pulses of 17 s, this value is much smaller than the real rest period, even so it was selected to achieve a clearer figure.

At the beginning of the simulation the ECB is discharged and the supercapacitor bank is charged to approximately 371 V, this value corresponds to almost 99% of the maximum voltage. When the pulse initiates, it takes a little more than 100 ms for the current of the TF coils to reach its reference (15000 A), the rectifier power supply immediately starts providing current to the coils and the CB. During the pulse the voltage of the supercapacitor bank fluctuates due to the voltage drop on its equivalent series resistance (ESR). The circuit oscillates between two states which was already illustrated in Figure 4.13, during the state 3 the CB is feeding the coils, thus the voltage drop, and during the state 2 the coils are disconnected from the CB. The minimum voltage of the supercapacitor bank, reached at the end of the first pulse, is 150.3 V which is enough to sustain the desired current intensity. When the pulse ceases, the ECB charges in 50 ms to approximately 780 V, and remains charged until the beginning of the next pulse. The rectifier power

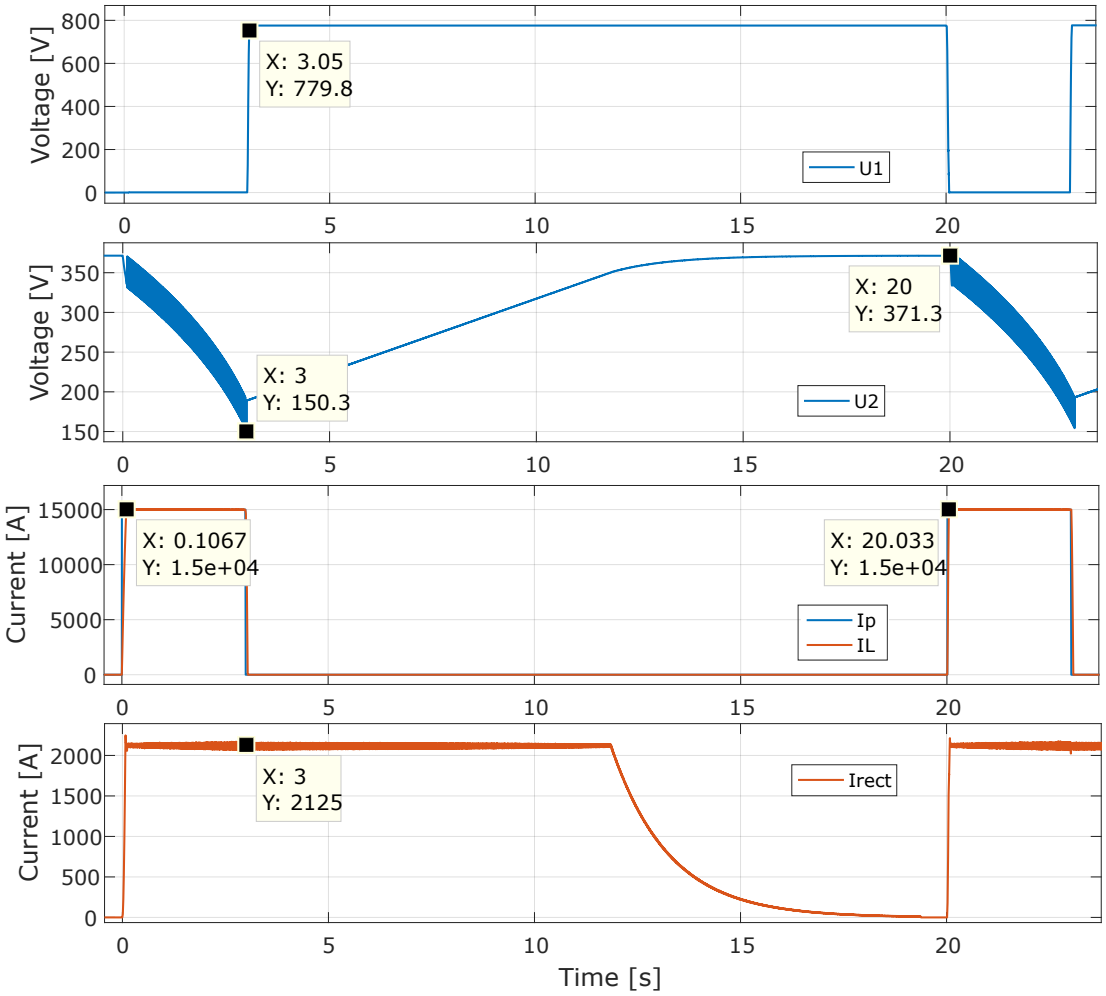

Figure 4.19: Main waveforms of the circuit for the modified rectifier power supply with auxiliary capacitor banks, considering a pulse of 15000 A with 3 s. Operation of the system and charging and discharging process of the capacitor banks.

supply keeps feeding current to the supercapacitor bank until its voltage reaches the reference value, near 371 V which is the maximum average voltage of the rectifier. The ripple of the output current of the rectifier depends on the value of the inductor L_rect, which is represented in Figure 4.17. The higher the inductance the less current ripple, in this case the inductance is 0.4 mH. This inductor assures that the current of the rectifier is enough stable for the PI controller to correctly adjust it. Finally, the ECB is discharged at the beginning of the next pulse which causes the current flowing through the coils to rise faster, about 33 ms.

If the desired current intensity of the pulse corresponds to a higher power demand than the limit of the rectifier power supply then the final voltage of the supercapacitor bank will be lower than the initial voltage, this is verified in Figure 4.19. On the other hand, if the desired current intensity is lower than 8500 A then the final voltage of the CB will be approximately equal to the initial, this is verified in Figure 4.20. This figure was obtained considering the same CBs and a pulse of 6000 A with 3 s, and a rest period of 7 s.

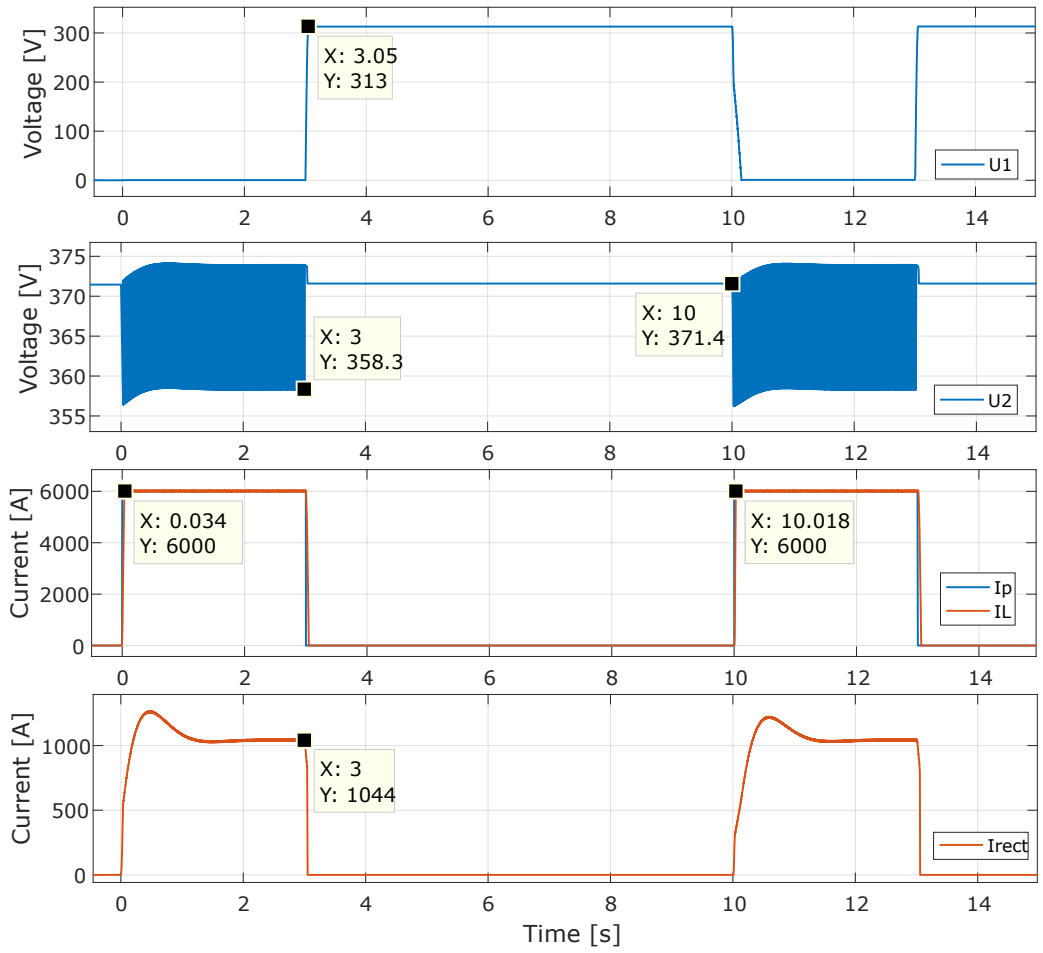

Figure 4.20: Operation and main waveforms of the circuit considering a pulse of 6000 A with 3 s.

The operation and the results are similar, however in this case the rectifier does not need to operate at maximum current during the pulse. As soon as the pulse ends the rectifiers ceases to

supply current because the CB is already charged to its nominal voltage.

4.5 Energy Recovery Upgrade of the Existing Power Supply (3rd Solution)

In this section, the possibility of adding a supplementary circuit to the 12-pulse rectifier power supply is assessed. The purpose of this complement is to recover the magnetic energy left in the TF coils, avoiding the re-injection of this energy into the public grid. As a result, it is possible to reuse the magnetic energy stored in the coils, on the tokamak, during the next pulse. Also, this solution has the potential to obtain better current rise and fall times. The circuits that will be presented for this solution were developed seeking to achieve the least possible changes on the existing system, while minimizing the number of semiconductors in the active current path to minimize on-state losses. The main configuration of the power supply is not modified, just the connection to the TF coils. The energy transfer between the coils and the CB happens within time intervals in the order of milliseconds, therefore it is required electrolytic capacitor cells. The process for sizing the ECB was covered in subsection 4.3.2.

4.5.1 Theoretical Circuit Schematics and Operation States

In order to connect the ECB to the TF coils it is required a circuit based on semiconductor devices, preferably with the minimum number of components needed, specially semiconductors in the active current path. The circuit must be able to operate in the first and fourth quadrant, which are characterised by positive current and positive and negative voltage respectively. The first circuit that was developed for this solution is represented in Figure 4.21 (a). It has only 2 diodes and 1 switch, this is the minimum number of semiconductor devices mandatory. The second circuit uses one more semiconductor switch which is represented in Figure 4.21 (b). However, it has the benefit of not having a diode in the main current path, this means that there is no semiconductor between the rectifier power supply and the TF coils, thus avoiding additional losses and voltage drop on the semiconductors. An important difference between the two converters is the fact that in the first circuit the capacitor discharges in series with the rectifier, but in the second circuit the capacitor is in parallel with the rectifier during the discharge. This last situation is problematic, therefore the second converter is not the best option.

Considering that the current of the inductor L is positive the first circuit operates in 3 states which are presented in Table 4.8. This table also expresses the voltage across the inductor with and without taking into consideration the voltage drop across the semiconductors.

Regarding the first circuit, the state 1 occurs when switch S is open and the voltage across the inductor is positive, as a result, the rectifier applies voltage to the inductor L. The state 2 occurs when switch S is open and the voltage across the inductor is negative, as a result, the voltage

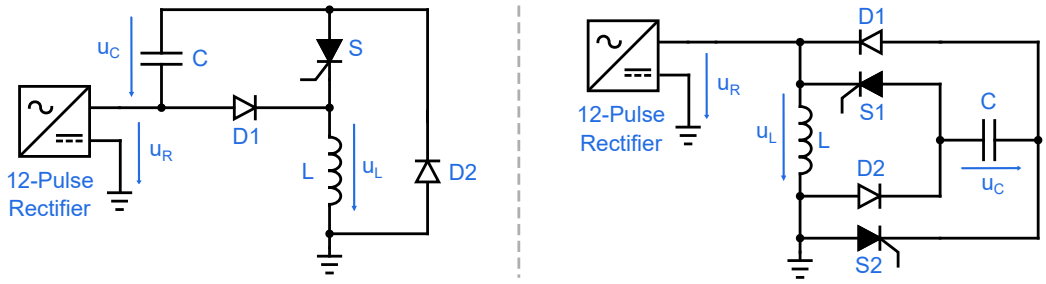

Figure 4.21: Circuit schematics used on the third solution: (a) minimum number of semiconductor devices; (b) without semiconductors in the main current path.

Table 4.8: Voltage across the inductor for all states of the first circuit.

State	**S**	u_L	u_L **without voltage drop**	u_L **with voltage drop**
1	OFF	≥ 0	$u_L = u_R$	$u_L = u_R - u_{D1}$
2	OFF	<0	$u_L = -u_C$	$u_L = -u_C - u_{D1} - u_{D2}$
3	ON	>0	$u_L = u_C + u_R$	$u_L = u_C + u_R - u_S$

of the capacitor C is equal to the negative voltage across the inductor L. During this state, the inductor charges the capacitor through the diodes (D1 and D2). The second state occurs when switch S is closed, as a result, the voltage applied to the inductor is equal to the sum of the voltage on the capacitor C and the voltage at the output of the 12-phase rectifier. It is important to note that the first circuit only operates correctly if the following condition is verified

$$u_C + u_R < 0 \tag{4.32}$$

This condition assures that the diode D2 conducts and thus the current flows through the right path of the circuit, allowing the inductor L to discharge to the capacitor C.

4.5.2 Rectifier Power Supply with an ECB System

The circuit schematic represented in Figure 4.21 (a) was implemented in Simulink and it is shown in Figure 4.22. The subsystem named 12_Pulse Rectifier comprises the existing power supply circuit, including the power transformers, the thyristors and the interphase reactors, this subsystem is represented in Figure 3.3. The capacitor C1 and the resistor Rc1 characterize the ECB which is sized based on the concepts presented in subsection 4.3.2. Taking into consideration that the power supply is limited to a maximum current intensity of 8500 A, and considering a maximum voltage for the capacitor bank of 800 V, the value obtained for the capacitance of the ECB is 187.5 mF. The component C1 is an ideal capacitor with the required capacitance and Rc1 is the ESR. In this case, the semiconductor switch (T) is a thyristor that conducts at the beginning of the pulse and turns off after the ECB as discharged to the TF coils.

This circuit was the first one to be implemented, however there are a few drawbacks to this

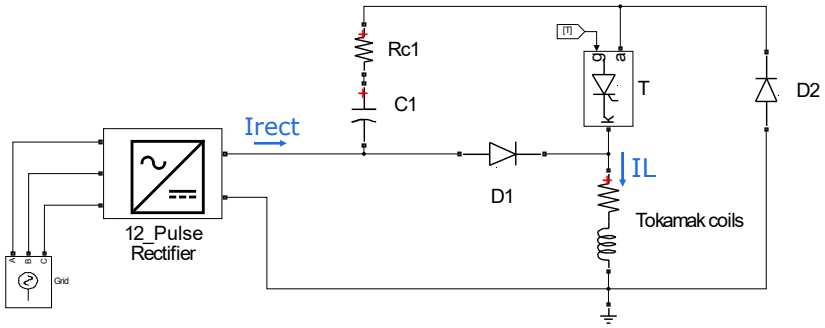

Figure 4.22: [Circuit 3.1] Implementation of the first circuit attempt with energy recovery.

approach. In order for the circuit to operate correctly the thyristors of the rectifier must enter a non-conducting state at the end of the pulse, thus blocking the current coming from the power supply to the TF coils allowing the state 2 (from Table 4.8) to take over. This is partially achieved by setting the trigger angles of the thyristor to 150 degrees, even so this is not enough. The condition (4.32) must be always verified for the diode D2 to conduct. If the ECB is not sized properly the voltage exceeds a certain value and the condition becomes invalid, consequently, the diode D2 turns off and the thyristors of the rectifier are forced to conduct. As a result, the current keeps circulating through the rectifier instead of the capacitor branch, and the energy left in the coils is still re-injected into the grid. This issue is represented in Figure 4.23 which illustrates the end of a pulse (recovery process). The waveforms of the voltage across the TF coils (UL) and the ECB (UC) are represented in Figure 4.23 (a). The relevant current waveforms are shown in Figure 4.23 (b), where Iref is the reference, Irect the output current of the rectifier and IL the current flowing through the TF coils. The voltage of the capacitor bank only reaches 96 V which in terms of efficiency corresponds to approximately 3 % of the magnetic energy left in the TF coils.

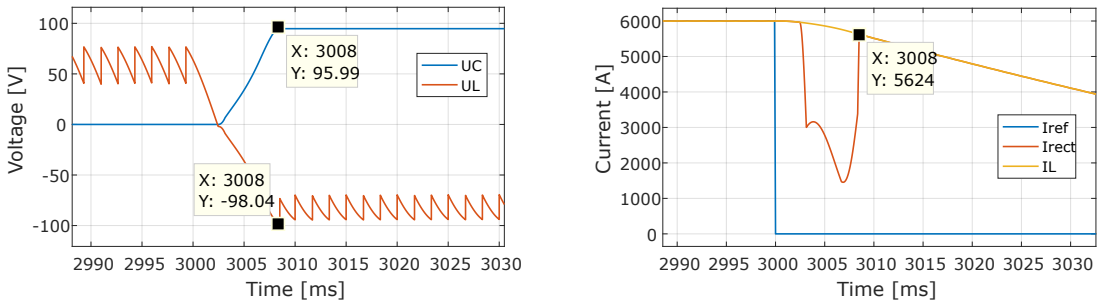

Figure 4.23: Waveforms at the end of a pulse for: (a) the voltage across the ECB and the coils; (b) pertinent currents. Circuit not operating properly.

For the condition (4.32) to remain true the ECB must have a high capacitance value, which reduces the final voltage that the ECB reaches. This is also an issue because by increasing the capacitance, the resistive losses during the recovery process increase. The time it takes for the energy transfer also increases which is verified by (2.17). This problem can be solved by adding an additional semiconductor switch in the main current path, in this case the most suitable one

is an IGBT. Since this switching device is connected in series with the rectifier and the TF coils, when the IGBT is turned off the rectifier ceases to supply current to the coils, allowing the current to flow entirely in the parallel recovery circuit. As a result, the magnetic energy left in the coils is discharged through this supplementary circuit instead of the rectifier. The circuit is represented in Figure 4.24 where the orange route is the main current path (a) and the blue route the recovery path (b).

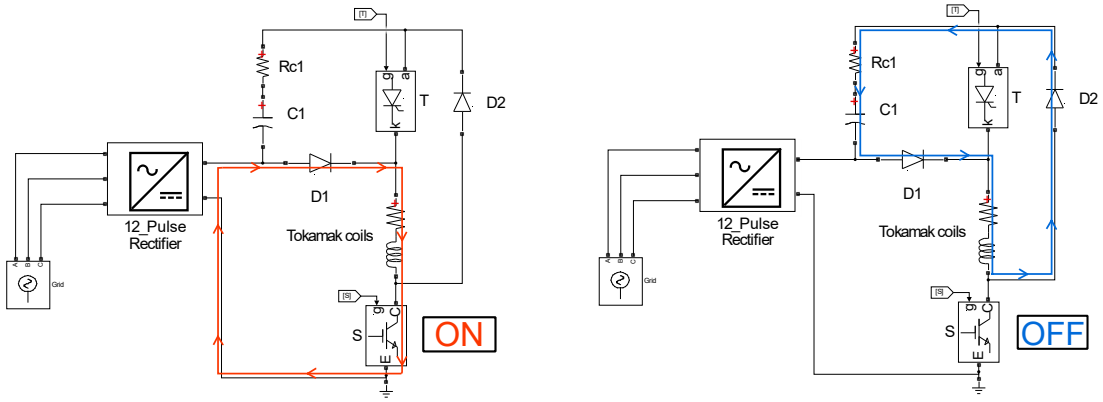

Figure 4.24: Current paths of the circuit with a semiconductor switch in series: (a) main current path; (b) recovery path.

Another pertinent concern is the magnetic energy left in the interphase reactors. Having a semiconductor switch in series that fully disconnects the rectifier power supply from the load, removing the only path for the current coming from the rectifier, causes a very high voltage spike due to the interphase reactors present within the circuit. When the current flowing through an inductor changes, the time varying magnetic field induces an electromotive force. Therefore, the magnetic energy stored in the interphase reactors must be discharge through other branch of the circuit. There are a few potential options to avoid this concern, the most reasonable are: storing the magnetic energy in a small capacitor bank or dissipating this energy in a resistor.

Using a Small Capacitor Bank and a Damping Resistor

The first solution that was implemented was placing a small capacitor bank in parallel at the output of the rectifier which is shown in Figure 4.25. Adding this branch to the circuit assures that the current flowing through the interphase reactors has a path to flow when the semiconductor switch (S) disconnects the rectifier from the TF coils.

The CB is establish with the capacitor C2 and the resistor Rc2. Adding a capacitor to the system results in a resonant circuit, however, the capacitance value is so little compared with the inductance that the waveforms of the circuit are just slightly affected. There is also a resistor in series with the CB, labeled Rd, which is responsible for damping the oscillations of the system, reducing the variation on the output current of the source. The current flowing through the coils remains identical, but the current at the output of the rectifier power supply starts having small

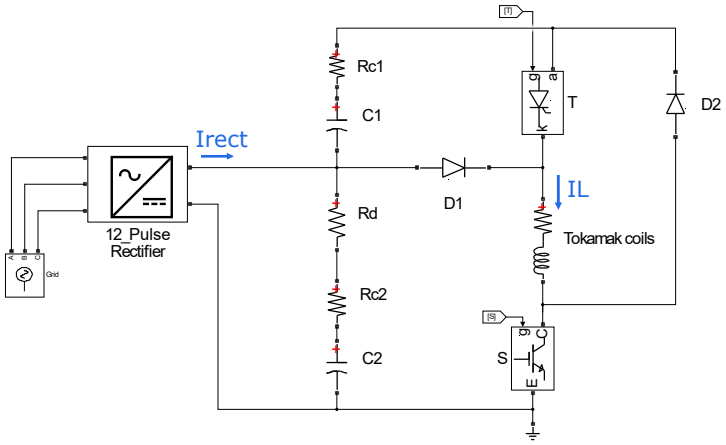

Figure 4.25: [Circuit 3.2] Implementation of the recovery circuit with an additional CB.

spikes due to the charging intervals of the capacitor, this distortion is represented in Figure 4.26 for a pulse of 6000 A. Where Iref is the current reference, Irect the current at the output of the rectifier and IL the current flowing through the TF coils. In this case, the pulse duration and the rest period were reduced to 2 s and 1 s respectively in order to obtain a clearer image. Figure 4.26 (a) shows a complete pulse and the start of another one after the ECB has been charged (at the end of the first pulse). Figure 4.26 (b) shows a zoomed portion of the steady section (flat top) of the pulse. This figure also demonstrates how much faster it is for the pulse to stabilize when the ECB is charged.

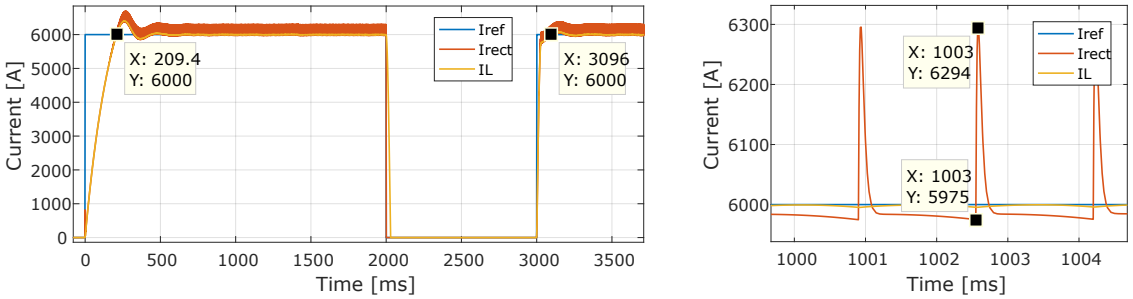

Figure 4.26: Current waveforms and current oscillation for: (a) the complete pulse; (b) a zoomed steady section of the pulse. Unwanted current spikes.

Regarding the capacitance of the capacitor bank (C2) the value used for the simulations was approximately 1 mF. The higher this value is the wider the current spikes represented in Figure 4.26 (b). Considering this capacitance value, the most suitable type of capacitors for this purpose are film capacitors. The value used for the damping resistor (Rd) was 80 mΩ. The higher this parameter is the lower the amplitude of these current spikes, which is beneficial, however the over-voltage at the end of the pulse is higher. This surge results from the discharge of the interphase reactors, if the value of the damping resistor is to great the voltage spike might harm the components. The power dissipation on the resistor during the steady section of the pulse with

6000 A is less than 300 W, nevertheless, the resistor must withstand the magnitude of the pulse current at the end of the pulse (surge).

Using a Thyristor and a Resistor

The second option to avoid the concern of the energy left in the interphase reactors is to dissipate it on a resistor, which is only connected to the circuit at the end of the pulse through a semiconductor switch. This alternative is apparently the best solution, considering it has the following advantages: the current and voltage waveforms during the pulse are not affected, the current spikes no longer exist, and there is no need for another capacitor bank. The only drawback to this solution is the requirement for another semiconductor device (thyristor), although this component would be much smaller than the other semiconductors, since this thyristor only conducts strong currents for a very small interval, less than 1 ms. Even thyristors with nominal current ratings below 1 kA are capable of addling current peaks of more than 10 kA for short periods of time (commonly less than 10 ms). The implementation of the circuit is represented in Figure 4.27.

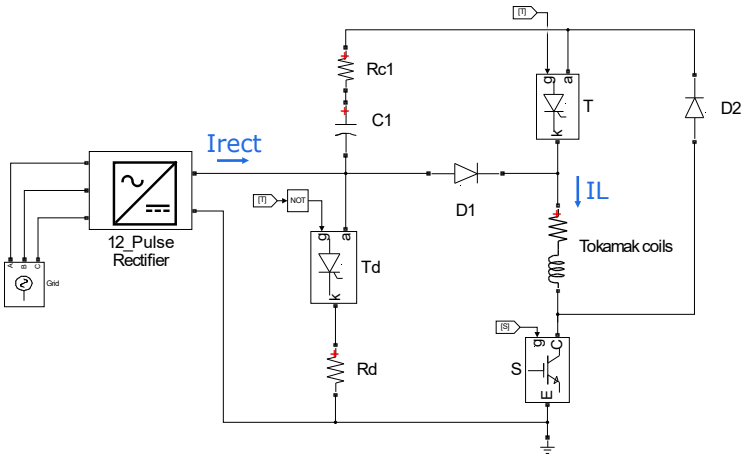

Figure 4.27: [Circuit 3.3] Implementation of the recovery circuit with an additional thyristor and resistor.

The extra thyristor is designated by Td and the resistor used to dissipate the energy is designated by Rd. The operation of the circuit is represented in Figure 4.28 for a pulse of 6000 A with 2s and a interval between pulses of 1s. As it was mentioned before these time values are only used to obtain a clearer image. The waveforms of the currents are shown in Figure 4.28 (a), and the denomination used is the same. During the pulse, the current at the output of the rectifier is the same current flowing through the coils, these two currents are only different at the end of the pulse when the semiconductor devices S and Td switch their operation state. As a result, the current flowing through the coils is redirected to the ECB to recover the magnetic energy left in the coils, and the current coming from the rectifier is redirected to the resistor Rd to dissipate the energy of the interphase reactors. The voltage at the terminals of the ECB (UC) and across the coils (UL) are also represented in Figure 4.28 (b). It is possible to verify that the capacitor bank

only charges at the end of the pulse reaching a voltage of 551.1 V which corresponds to approximately 84 % of the energy stored in the TF coils for a pulse of 6000 A, this section is represented with more detail in Figure 4.29 (a). At the beginning of the next pulse the ECB is already charged, therefore, the voltage applied to the coils reaches a peak value of 642 V since the capacitor bank discharges in series with the rectifier. As a result, the current rise time is shortened a lot which is shown in Figure 4.28 (a). The time it takes for the current flowing through the coils (IL) to reach the reference value (in this case 6000 A) is 97 ms when the ECB is charged and 209 ms when it is discharged. However, this difference is significantly greater if it is considered 96 % of the current reference value instead. When the ECB is charged, it takes approximately 27 ms to reach 96 % of the reference value, which is shown in Figure 4.29 (b), this is also the time it takes for the capacitors to discharge. In comparison, when the ECB is discharged it takes 193 ms for the current to reach the same value, which is around 7 times slower. Another benefit of this circuit is the reduction of the over-current at the beginning of the pulse. When the ECB is discharged the peak current is 6403 A, however when it is charged the peak drops to 6071 A.

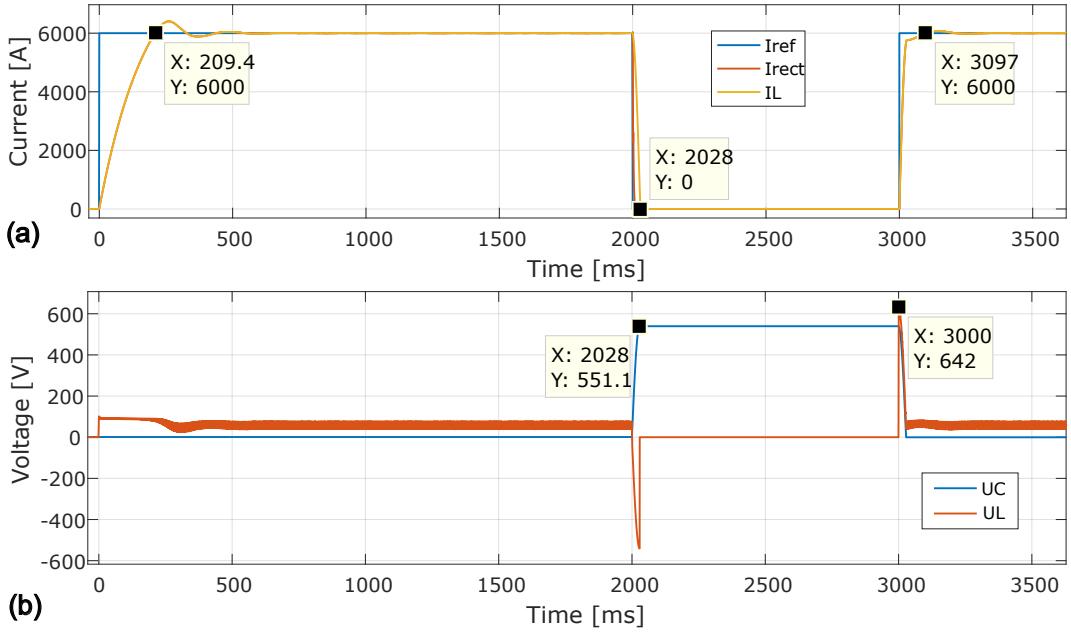

Figure 4.28: Waveforms of the circuit for a pulse of 6000 A: (a) main currents; (b) voltage of the ECB and voltage applied to the coils. Waveforms are only affected during the recovery process.

Finally Figure 4.29 (c) represents the current flowing through the resistor Rd (IRd) at the end of the pulse, and the current flowing through the capacitor bank (IC).

From this figure it is verified that the thyristor Td only conducts current with intensity above 1 kA for a very brief period, less than 1 ms. Contrarily, the diode D2 conducts for the entire charging process of the capacitor, which takes 28 ms. In order to size the resistor Rd it is necessary to compute how much energy it is dissipated in it. This can be computed by integrating the square of the signal IRd represented in Figure 4.29 (c) and multiplying by the value of the resistor. In this

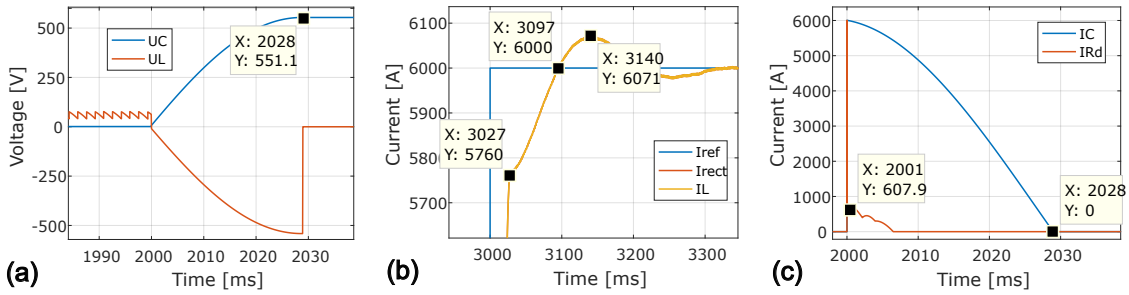

Figure 4.29: Sections of the pulse represented with more detail: (a) voltage of the ECB and the coils; (b) current at the beginning of the second pulse; (c) current at the end of the pulse.

case the resistance used for Rd was 0.1 Ω, as a result, for a pulse of 6000 A the peak voltage across the resistor is 600 V which is near the maximum voltage applied to the coils, and the energy dissipated is approximately 150 J. When the rectifier is operating at maximum current (8500 A) the energy dissipated on this resistor is approximately 340 J.

The operation of this circuit was also analysed considering other pulses. Figure 4.30 shows the waveforms of the currents (a) and voltages (b) for a pulse of 8500 A.

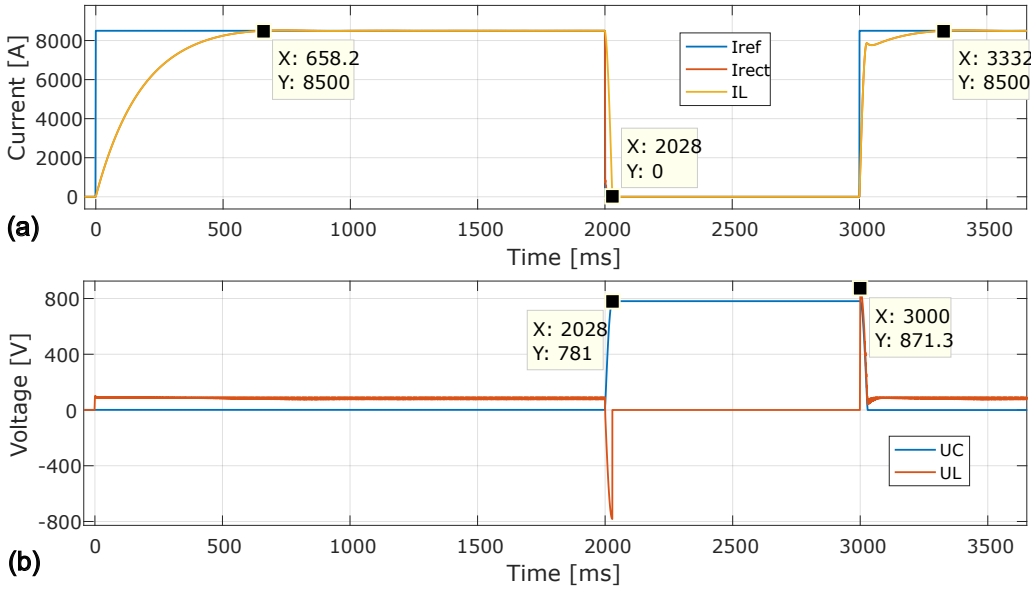

Figure 4.30: Waveforms of the circuit for a pulse of 8500 A: (a) main currents; (b) voltage of the ECB and voltage applied to the coils.

It is crucial to examine the behavior of the circuit for the limited maximum current which is 8500 A. The signals represented in Figure 4.30 are the same ones that were represented in Figure 4.28. Take notice that the time it takes for the coils to discharge to the ECB is the same for both cases represented in Figure 4.28 and Figure 4.30. It takes 28 ms for the ECB to charge. This is expected since according to (2.17) the discharge time is independent of the current intensity. Considering the capacitance of the ECB (187.5 mF) and the inductance of the TF coils (1.88 mH)

the discharge time obtained using (2.17) is approximately 29 ms, which is very close to the value obtained from the simulations (28 ms).

4.6 Semiconductor Modules and Power Losses on Devices

The circuits that were presented in this chapter rely on its semiconductor devices. The selection of the semiconductor types was made considering the concepts provided in section 2.5 of the state-of-the-art. All simulations were conducted considering the real parameters of the semiconductor devices, provided on their datasheets. Take notice that all the circuit schematics that were analysed were represented using a single symbol per semiconductor device. In reality, this is not the case, each semiconductor symbol represents a module which is often composed by more than one semiconductor component in parallel. The values of the parameters of the semiconductor devices used for the simulations, resulted from the association of this components in parallel, therefore, the values correspond to equivalent parameters. The number of semiconductor devices that must be connect in parallel (Np_{sd}) per module to withstand the current intensity is given by

$$Np_{sd} = ceil\left(\frac{I_p}{I_r}\right) \tag{4.33}$$

Where I_p is the current intensity of the pulse, I_r is the current rating of the semiconductor device and $ceil$ is the smallest integer greater than or equal. This equation is used to compute the number of diodes and IGBTs that are required in parallel. However, with thyristors the equation (4.33) is slightly modified. By analysing the circuit schematics it is verified that the thyristors never appear on the main current path. As a result, these devices only conduct current with an intensity higher than its current rating during a very short interval. If this period is smaller than 10 ms, then instead of using the rated current (I_r) on (4.33) it is used the surge current (I_s) which is much superior and thus leads to a smaller number of components in parallel. The values of the parameters of the semiconductor devices are represented in Table 2.8.

Power Losses on the Semiconductor Devices

Regarding the power losses on the semiconductor devices, there are two types of losses: conduction and switching losses. The first one results from the current flowing through a switch or diode when it is forward biased, due to the internal resistance of the component. The conduction losses (P_{on}) on a semiconductor device are given by

$$P_{on} = V_{on}I_{av} + R_{on}I_{RMS}^2 \tag{4.34}$$

Where is V_{on} is the forward voltage during conduction, I_{av} the average value of the current, R_{on} is the internal resistance of the component and I_{RMS} the root mean square of the current. If

the current is DC then the average value is equal to the RMS. The switching losses ($P_{switching}$) happen every time a component switches on or off, and they are given by

$$P_{switching} = n_{on}E_{on} + n_{off}E_{off} \tag{4.35}$$

Where n_{on} is the number of times the switch turns on, E_{on} the turn on energy lost per commutation, n_{off} the number of times the switch turns off, E_{off} the turn off energy lost per commutation. Generally, the values of n_{on} and n_{off} are equal.

Regarding the circuits presented, it is important to make a distinction between the main current path and the recovery path. The main path includes the TF coils, its source, and every component between them. The recovery path is the part of the circuit used to transfer energy between the ECB and the TF coils, thus the current only flows through it during the recovery process or at the beginning of the next pulse. The semiconductors on the main path must conduct during the full duration of the pulse, however, the semiconductor devices on the recovery path only conduct for a few milliseconds, thus they can be smaller than the others.

5

Conclusions

The present work addresses the design of an ESS for the fusion reactor named ISTTOK. The ESS concedes the capability to recover the magnetic energy left in the TF coils, but may also feed the coils. There are three distinct solutions that stand out, each one having strong advantages but also drawbacks. The most promising options were developed and analysed to determine the most suitable one. In this chapter, these solutions will be compared based on the results that were obtained before, its benefits and the costs related with the materials and equipment required. The circuits strive to minimize the number of capacitor cells and semiconductor devices needed, as they are the most expensive components.

The supercapacitor power supply with an additional DC source was the first option studied. This solution consists of a supercapacitor power supply able to replace the exiting 12-pulse rectifier. This ESS has a supercapacitor bank that charges between the pulses using a relatively low power DC source, and discharges during the pulse. This option is capable of reducing the contracted power tariff since the source of the TF coils becomes the CB instead of the rectifier power supply. As a result, the grid provides the energy required for the pulse throughout the entire rest period, rather than solely during the pulse. By spreading the energy demand throughout the operation cycle, it is possible to decrease the contracted power tariff from about 1 MVA to few kVA, depending on the interval between pulses. For example, considering a rest period of 15 min confers a power demand from the grid of approximately 5 kVA. Depending on the selected CB, it is possible to increase the intensity of the current that flows through the TF coils.

There are a few considerations to be accounted for in this option. The solution requires many CCs because the CB must provide all the energy needed for the pulse, which is more than 1 MJ. Table 4.2 represents the parameters and results, including the number of supercapacitor cells, for a few CBs that were design. It is also required a DC power supply to charge the capacitors, either a new one or the existing rectifier. As a result, the first option has substantial costs involved.

The modified rectifier power supply with auxiliary capacitor banks was the second option analysed. This solution is a combination between the existing 12-pulse rectifier and a supercapacitor power supply. The configuration of the rectifier is slightly modified in order to obtain a higher output voltage. The power supply feeds the TF coils together with the supercapacitor bank, as a result, this CB does not need to be as large as the one used in the supercapacitor power supply with an additional DC source (first option). The third solution was illustrated in section 4.4 considering all the three-phase rectifiers in series, even so, it is possible to only connect the two six-phase halves of the rectifier in series. In comparison with the other configuration, this results in an output voltage with half the amplitude and an output current with twice the intensity. This setup is better for pulses with a current intensity lower than 13 kA and optimal around 10 kA. The configuration with all the rectifiers in series is better for pulses with a current intensity higher than 13 kA and optimal around 15 kA, which was the value used for the simulations on subsection 4.4.4.

The modified rectifier power supply with auxiliary capacitor banks is adequate if the intention

is to increase the maximum intensity of the current supplied to the TF coils. Even though the supercapacitor power supply with an additional DC source (first solution) is capable as well, this option allows the 12-pulse rectifier to assist the CB. It is also possible to decrease the contracted power tariff, since the power supply works in conjunction with the supercapacitor bank.

The energy recovery upgrade of the existing power supply was the third option studied. This solution is an upgrade to the existing rectifier power supply, which consists in an additional circuit that complements the operation of the TF system. The purpose of this upgrade is to store the magnetic energy left in the coils at the end of the pulse in an electrolytic capacitor bank (ECB), so it can be later reused in the tokamak. The efficiency of the recovery process (energy transfer from the TF coils to the ECB) is approximately 84 %. At the beginning of the next pulse, the ECB discharges through the coils, causing a high voltage to be applied to its terminals, and thus energizing them very quickly. This solution is also capable of avoiding the re-injection of the energy left into the public grid.

Unlike the supercapacitor power supply with an additional DC source, in this case the CB only stores the remaining magnetic energy in the TF coils which is much less than the energy required for the pulse. Therefore, the number of cells needed in comparison is considerably smaller. This option is the least demanding in terms of components.

It is important to note that the ECB used in the energy recovery upgrade of the existing power supply, can be also included in the first and third solution. This CB makes the system very fast to respond because it makes it possible to apply a higher voltage to the TF coils. As a result, the rise and fall time of the current is reduced.

Lastly, the solutions and the corresponding circuits that were presented in this thesis are illustrated in Table 5.1. This table shows a resumed comparison between the topologies that were analysed, presenting the advantages and disadvantages of each. Regarding Table 5.1 the column named SCB indicates if the circuit has a supercapacitor bank, the ECB indicates if the circuit has an electrolytic capacitor bank, the columns with the names of the semiconductor devices indicate how many of these components the circuit has. The column named Extra Elements indicates if the circuit has additional components, the circuit 3.3 has an extra thyristor this element is represented with ”+ 1” in the number of thyristors because its power rating is much lower than the other thyristor.

In summary, the fist solution is the most adequate to reduce the contracted power tariff, the second solution the most appropriate to increase the intensity of the current flowing though the coils, and the third solution the most appropriate to only reuse the energy left in the coils. The most economic option is the circuit 3.1, because it requires less semiconductor devices and capacitor cells. The best solution disregarding the economic aspect is the circuit 1.2, since it is capable of reducing the power demand from the grid, as well as capable of obtaining better waveforms and even able to increase the intensity of current if that is the intention.

Future Work

Regarding the future work, there are a few subjects that would be interesting to study. Firstly, it would be useful to analyse the possibility of reusing the magnetic energy left in the TF coils in another electromagnetic system of the tokamak besides the TF system, like the poloidal field or the ohmic heating system. For example, the ohmic heating system also uses an ECB to maintain the plasma state until the transformer yoke is saturated. On the other hand, using this energy in other systems besides the TF might have more losses during the transfer processes.

Secondly, it would be appropriate to evaluate the installation of the energy storage system, taking into consideration the predicted dimensions and requirements, and how to establish the connections. Also, in order to correctly associate the supercapacitor cells it is required a capacitor management system to maintain a balance between the voltage across all cells.

The total cost of the ESS must be estimated at the beginning of the project to re-evaluate the viability of the system. Furthermore, it must be taken into account the costs related to the re-injection of the energy into the public grid. Only then, it is possible to determine accurately if the solution is beneficial.

Table 5.1: Comparison between the different topologies that were analysed.

Solution	Circuit	SCB	ECB	IGBTs	Diodes	Thyristors	Extra Elements	Advantages	Drawbacks
1st Supercapacitor Power Supply with Additional DC Source	1.1	Yes	No	2	2	0	Power Supply	Reduces contracted power tariff; Potential to increase maximum current.	Large SCB, requires more cells; Requires new power supply to charge SCB.
	1.2	Yes	Yes	2	2	0	Power Supply	Reduces contracted power tariff; Better current rise and fall times; Potential to increase maximum current.	Large SCB, requires more cells; Requires a new power supply to charge SCB.
2nd Modified Rectifier Power Supply with Auxiliary Capacitor Banks	2	Yes	Yes	2	2	0	Modifications on the rectifier.	Uses the existing rectifier as the SCB charger and assists it during the pulse; Better current rise and fall times; Potential to increase maximum current.	Requires modifications on the existing rectifier power supply.
3rd Energy Recovery Upgrade of the Existing Power Supply	3.1	No	Yes	0	2	1	No	Lowest cost option;	Lowest efficiency of the recovery process.
	3.2	No	Yes	1	2	1	Small CB, Resistor.	Low cost option; Better current rise and fall times.	Requires an additional small CB and a resistor; Slightly affects the waveforms.
	3.3	No	Yes	1	2	1 + 1	Small Thyristor, Resistor.	Low cost option; Better current rise and fall times.	Requires an additional small Thyristor and resistor (inexpensive).

Bibliography

[1] S. Mirnov, “Tokamak evolution and view to future,” *Nuclear Fusion*, vol. 59, 11 2018.

[2] M. Aneke and M. Wang, “Energy storage technologies and real life applications – a state of the art review,” *Applied Energy*, vol. 179, pp. 350–377, 10 2016.

[3] M. Güney and Y. Tepe, “Classification and assessment of energy storage systems,” *Renewable and Sustainable Energy Reviews*, vol. 75, 11 2016.

[4] Fission and fusion: What is the difference? Acessed in November 2020. [Online]. Available: https://www.energy.gov/ne/articles/fission-and-fusion-what-difference

[5] H. R. Mirzaei and R. Amrollahi, “Design, simulation and construction of the taban tokamak,” *Plasma Science and Technology*, vol. 20, p. 045103, 04 2018.

[6] V. A. Glukhikh, “Chapter 1 - engineering and physical principles of the magnetic fusion reactor operation,” in *Fundamentals of Magnetic Thermonuclear Reactor Design*, 2018, pp. 1 – 5.

[7] Tokamak isttok. Acessed in November 2020. [Online]. Available: https://www.ipfn.tecnico.ulisboa.pt/cfn/pt/Prj_Tokamak_main_1.html

[8] Isttok - wiki. Acessed in November 2020. [Online]. Available: https://isttok.tecnico.ulisboa.pt/isttok.daemon/index.php?title=ISTTOK_-_Wiki

[9] H. Fernandes, J. Cabral, C. Varandas, and C. Silva, “20 years of isttok tokamak scientific activity,” *Presented at the 24th IAEA Fusion Energy Conference. San Diego, USA*, p. 7, 2012.

[10] J. Santana, V. Anunciada, V. Líbano Monteiro, J. C. Lameira, C. Varandas, H. Fernandes, J. Sousa, and C. Freitas, “One megawatt supply for tokamak isttok,” *ELECTRICIDADE, N° 309*, pp. 94–105, 03 1995.

[11] F. Silva, *Electrónica Industrial, Fundação Calouste Gulbenkian*, 1998.

[12] S. Koohi-Fayegh and M. Rosen, “A review of energy storage types, applications and recent developments,” *Journal of Energy Storage*, vol. 27, p. 101047, 02 2020.

[13] A. Dehghani-sanij, M. Dusseault, E. Tharumalingam, and R. Fraser, “Study of energy storage systems and environmental challenges of batteries,” *Renewable and Sustainable Energy Reviews*, vol. 104, pp. 192–208, 04 2019.

[14] T. Aljohani, “The flywheel energy storage system: A conceptual study, design, and applications in modern power systems,” *International Journal of Electrical Energy*, 01 2014.

[15] M. Khodaparastan and A. Mohamed, “Flywheel vs. supercapacitor as wayside energy storage for electric rail transit systems,” *Inventions*, vol. 4, p. 62, 10 2019.

[16] H. TOODEJI, “A developed flywheel energy storage with built-in rotating supercapacitors,” *TURKISH JOURNAL OF ELECTRICAL ENGINEERING COMPUTER SCIENCES*, vol. 27, pp. 213–229, 01 2019.

[17] N. Nitta, F. Wu, J. Lee, and G. Yushin, “Li ion battery materials: Present and future,” *Materials Today*, vol. 18, 11 2014.

[18] R. Bavithra and B. Abarna, “Performance analysis of electrolytic and film type capacitor,” *International Journal of Students’ Research in Technology Management*, vol. 3, p. 425, 10 2015.

[19] J. Schnack, S. Bruckner, H. Suncksen, U. Schümann, and R. Mallwitz, “Analysis and optimization of electrolytic capacitor technology for high frequency integrated inverter,” *IEEE Transactions on Components, Packaging and Manufacturing Technology*, vol. PP, pp. 1–1, 05 2021.

[20] Britannica, semiconductor. Acessed in April 2021. [Online]. Available: https://www.britannica.com/science/semiconductor

[21] Different types of semiconductor devices. Acessed in June 2021. [Online]. Available: https://www.electronicshub.org/types-of-semiconductor-devices/

[22] I. Jiya and R. Gouws, “Overview of power electronic switches: A summary of the past, state-of-the-art and illumination of the future,” *Micromachines*, vol. 11, p. 1116, 12 2020.

[23] P. Pawar, G. Kumar, and A. Patil, “Study of semiconductor switches for electromagnetic launcher,” pp. 1–5, 08 2016.

[24] Series resonance circuit. Acessed in August 2021. [Online]. Available: https://www.electronics-tutorials.ws/accircuits/series-resonance.html

[25] M. Elborhamy, E. E. Rashad, and I. Sobhy, “Floquet analysis of linear dynamic rlc circuits,” *Open Physics*, vol. 18, 07 2020.

[26] L. Ries and M. Heldwein, “Current balancing control methods using advanced carrier-based modulation for five-level current source rectifiers,” *IEEE Transactions on Power Electronics*, vol. PP, pp. 1–1, 03 2020.

[27] R. Bhide and S. V. Kulkarni, “Analysis of parallel operation of converters with interphase transformer,” *2006 India International Conference on Power Electronics*, pp. 193–196, 2006.

[28] F. Silva and S. Pinto, *Control Methods for Switching Power Converters*, 12 2007, pp. 935–998.